1. Symmetry

1.1 Model Surfaces

1.1.1 Surface Versus Bulk

Every real solid is bounded by surfaces. Nonetheless, the model of an infinite solid which neglects the presence of surfaces works very well in the case of many physical properties. The reason is, firstly, that one usually deals with properties, such as transport, optical, magnetic, mechanical or thermal properties, to which all the atoms of the solid contribute more or less to the same extent, and, secondly, that there are many more atoms in the bulk of a solid sample than at its surface, provided the solid is of macroscopic size. In the case of a silicon cube of 1 cm^3, for example, one has 5×10^{22} bulk atoms and 4×10^{15} surface atoms.

The surface atoms are only visible in surface sensitive experimental techniques or by studying properties or processes which are determined by surface atoms only. Among them are phenomena like crystal growth, adsorption, oxidation, etching or catalysis. They cannot be described by the model of an infinite solid. However, there are also effects which are determined by the interplay of bulk and surface (or, more strictly speaking, the interface). For instance, the channel of the carrier transport in field-effect transistors is determined by the surface (interface) states as well as the bulk doping. In one of the first theoretical approaches to the field effect, Bardeen [1.1] applied the premise of charge neutrality at the surfaces/interfaces. This condition means that in thermal equilibrium the surface band bending adjusts in such a way that the net charge in surface states is balanced by a space charge below the surface of the semiconductor forming the main part of the electrical device.

1.1.2 The Surface as a Physical Object

Under normal conditions, i.e., atmospheric pressure and room temperature, the real surface of a solid is far removed from the ideal systems desirable in physical investigations. A freshly prepared surface of a material is normally very reactive toward atoms and molecules in the environment. All kinds of particle adsorption – from strong chemisorption to weak physisorption – give rise to an adlayer on the topmost atomic layers of the solid. One example

is the immediate formation of an extremely thin oxide layer on a freshly cleaved silicon crystal. Usually the chemical composition and the geometrical structure of such a contamination adlayer are not well defined.

As an object of physical investigations a well-defined surface has to be prepared on a particular solid, in a special preparation process, under well-defined external conditions. Such a solid could be a crystalline material, a single crystal or a crystalline film deposited by epitaxy in a well-controlled way. A rather clean surface of such a crystalline system might also be prepared as an electrode surface in an electrochemical cell, or a semiconductor surface in a reactor where vapor phase epitaxy (VPE) is performed at standard pressure conditions and at elevated temperature. However, the processes of the underlying methods and the results are rather complex and difficult to characterize. The simplest ways to prepare a solid surface should happen in ultrahigh vacuum (UHV), i.e., at ambient pressure lower than 10^{-8} Pa (about 10^{-10} torr). There are essentially three ways to manufacture clean surfaces under UHV conditions:

i. Cleavage of brittle materials in UHV. Of course, only surfaces which are cleavage planes of the crystal can be made in this way.
ii. Treatment of imperfect and contaminated surfaces of arbitrary orientation by ion bombardment and thermal annealing (IBA), generally in several cycles. There are no limitations to certain materials and to certain crystallographic orientations.
iii. Epitaxial growth of crystal layers (or overlayers) by means of evaporation or molecular beam epitaxy (MBE).

Obviously, a smooth and clean surface cannot be realized in the ideal form, but rather only to some approximation. Any real surface will exhibit irregular deviations from perfect smoothness and purity despite the care taken in its preparation. An illustration of such a surface is given in Fig. 1.1. In reality a surface consists of a number of irregular portions of parallel surface lattice planes which are displaced vertically by one or more lattice plane separations with respect to each other. Atomic steps occur at the bound-

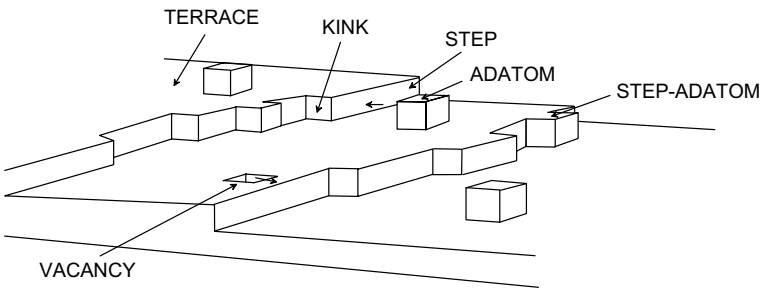

Fig. 1.1. Illustration of structural imperfections of crystal surfaces. Atoms and their electron shells are indicated by little cubes.

aries of these lattice-plane portions which in this context are called terraces. The steps may exhibit kinks. In addition to terraces, steps and kinks, other structural irregularities may occur which can be subsumed under the term 'surface roughness'. Adatoms and vacancies belong to this category, as do complexes of these simple defects. In the case of surfaces of compound crystals quite often atoms of one of the contributing elements are depleted more than those of the other which results in an enrichment of the latter and in a non-stoichiometry at the surface. The most significant form of chemical disturbance of surfaces, which applies both to compound and elemental crystals, is the contamination by impurities or adatoms of another species. The impurity atoms or adatoms may be situated at regular or nonregular sites of the surface lattice plane, at locations above and slightly below it.

1.2 Two-Dimensional Crystals

A complete characterization of a solid surface requires knowledge of not only atoms of 'what species' are present but 'where' they are. Just as in the bulk, it is not that the atomic coordinates as such are of much direct interest. Rather, besides the chemical nature of the atoms their geometrical arrangement governs the electronic, magnetic, optical, and other properties of surfaces.

1.2.1 Lattice Planes of Bulk Crystals

A geometrical construction which is of particular significance in describing crystal surfaces is that of a *lattice plane*. Lattice planes are usually denoted by *Miller indices* (hkl) where h, k, l are the integer reciprocal axis intervals given by the intersections of the lattice planes with the three crystallographic axes. They have a simple meaning in the case of rectangular crystal systems, e.g., the cubic system. The symbol (100), for example, denotes lattice planes perpendicular to the cubic x-axis, (111) means lattice planes perpendicular to the body diagonal in the first octant of the cubic unit cell, and (110) denotes the lattice planes perpendicular to the face diagonal in the first quadrant of the xy-plane of the cubic unit cell. Usually, the collection of such planes that are equivalent by symmetry is labeled $\{hkl\}$. Thus $\{100\}$ stands for the collection (100), $(\bar{1}00)$, (010), $(0\bar{1}0)$, (001) and $(00\bar{1})$, if these planes are equivalent. The bar notation $\bar{1}$ indicates the corresponding negative coefficient. In the case of trigonal and hexagonal lattices, four crystallographic axes are considered, three instead of two perpendicular to the c-axis. The lattice planes are then characterized by four indices $(hkil)$ instead of three. The first three, however, are not independent of each other. In fact $h + k + i = 0$. The fourth axis (corresponding to the index l) is perpendicular to the hexagonal basal plane. The $(hkil)$ are sometimes termed *Bravais indices*.

A particular geometrical plane can also be characterized by its normal direction

$\boldsymbol{n} = \tilde{\boldsymbol{n}}/|\tilde{\boldsymbol{n}}|$.

In the case of lattice planes it is convenient to relate it to a linear combination

$$\tilde{\boldsymbol{n}} = \frac{1}{2\pi}\left[h\boldsymbol{b}_1 + k\boldsymbol{b}_2 + l\boldsymbol{b}_3\right] \tag{1.1}$$

of the primitive vectors $\boldsymbol{b}_j$ ($j = 1, 2, 3$) of the reciprocal lattice with the integer coefficients h, k, and l. The vectors $\boldsymbol{b}_j$ are directly related to the primitive lattice vectors $\boldsymbol{a}_i$ ($i = 1, 2, 3$) by the relation

$$\boldsymbol{a}_i \cdot \boldsymbol{b}_j = 2\pi\delta_{ij}. \tag{1.2}$$

Apart from the case of primitive Bravais lattices, they are different from the crystallographic axes. Anyway, a lattice plane can be characterized by the Miller indices (hkl) and, hence, a normal parallel to the vector $\boldsymbol{G}_{hkl} = h\boldsymbol{b}_1 + k\boldsymbol{b}_2 + l\boldsymbol{b}_3$ of the reciprocal lattice. However, as a consequence of relation (1.2) the Miller indices depend on the particular choice of the primitive vectors of the Bravais lattice.

Miller indices are simplest to work with in simple cubic (sc) Bravais lattices, since the reciprocal lattice is also simple cubic and the Miller indices are the coordinates of a vector normal to the plane in the obvious Cartesian coordinate system. As a general rule, face-centered cubic (fcc) and body-centered cubic (bcc) Bravais lattices are described in terms of conventional cubic cells, i.e., as sc lattices with bases. Since any lattice plane in a bcc or fcc lattice is also a lattice plane in the underlying sc lattice, the same elementary cubic indexing (hkl) can be used to specify lattice planes. This agreement simplifies a variety of considerations for a lot of materials. Many important metals consisting only of one element crystallize within the cubic crystal system. Also many elemental and compound semiconductors or strongly ionic compounds form diamond, zinc-blende, or rocksalt crystals which also belong to the cubic crystal system.

The Miller indices of a plane have a geometrical interpretation in real space. Therefore, a similar convention is used to specify directions in the direct lattice, but to avoid confusion with the Miller indices (directions in the reciprocal lattice) square brackets are used instead of parentheses. For instance, the body diagonal of a sc cubic lattice lies in the [111] direction and, in general, the lattice point $h\boldsymbol{a}_1 + k\boldsymbol{a}_2 + l\boldsymbol{a}_3$ lies in the direction $[hkl]$ from the origin. In the cubic case $[hkl]$ defines the normal direction of the plane (hkl). The collection of such directions that are equivalent by symmetry is labeled $\langle hkl\rangle$. This holds in principle also for non-cubic Bravais lattices. However, in general the direction $[hkl]$ is not perpendicular to the plane (hkl).

The property of the vector $\boldsymbol{G}_{hkl} = h\boldsymbol{b}_1 + k\boldsymbol{b}_2 + l\boldsymbol{b}_3$ of the reciprocal lattice can be proven characterizing the lattice planes by all possible Bravais lattice points

$$\boldsymbol{R}_l = \sum_{i=1}^{3} n_{li}\boldsymbol{a}_i \tag{1.3}$$

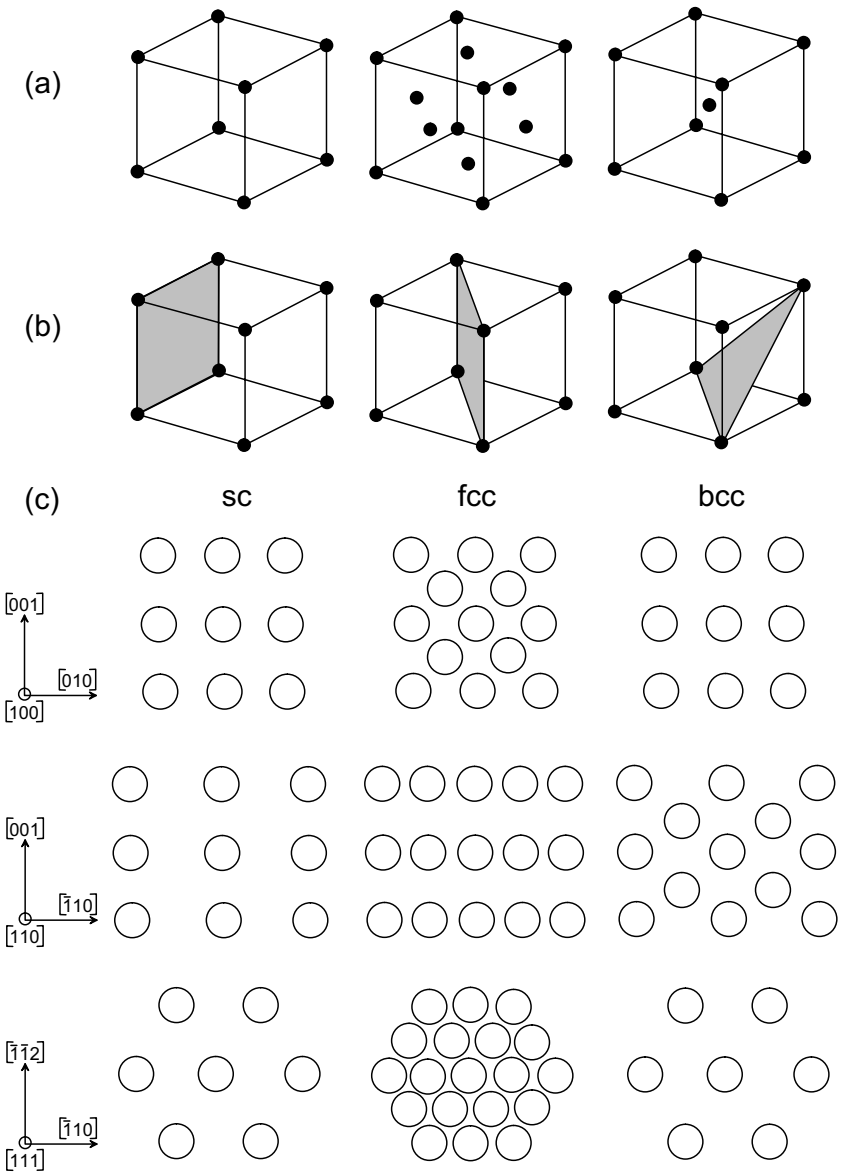

Fig. 1.2. (a) Cubic Bravais lattices sc, fcc, bcc; (b) low-index planes (100), (110), (111) in a sc cell; and (c) low-index planes resulting from cubic lattices. Bravais lattice points are indicated as dots (a,b) or spheres (c).

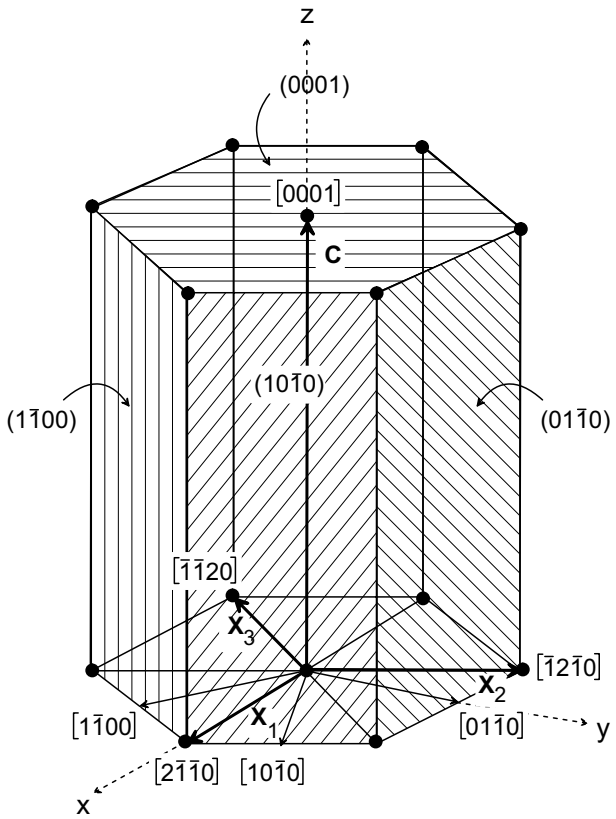

Fig. 1.3. Characteristic planes in a hexagonal Bravais lattice. Certain directions in this lattice are also indicated. The vectors $\boldsymbol{x}_1$, $\boldsymbol{x}_2$ (or $\boldsymbol{x}_3$), and $\boldsymbol{c}$ can be identified with the primitive Bravais lattice vectors. The directions $[2\bar{1}\bar{1}0]$, $[01\bar{1}0]$, and [0001] represent the hexagonal Cartesian coordinate system.

with integers n_{li} $(i = 1, 2, 3)$. The index l characterizes the infinite family of parallel planes in a certain distance from each other. The plane $l = 0$, which contains the zero point, may afterwards be identified with the surface of semi-infinite space. This is demonstrated in Fig. 1.2 for the low-index surfaces of sc, fcc, and bcc Bravais lattices (or monatomic metals crystallizing within these structures). In the case of a hexagonal Bravais lattice such lattice planes are indicated in Fig. 1.3. In practice, it is only in the description of non-cubic crystals that one must remember that the Miller indices are the coordinates of the normal in a system given by the reciprocal lattice, rather than the direct lattice. For that reason, sometimes for simplicity the Miller indices $(hkil)$ are also used to characterize the normal directions as done in Fig. 1.3.

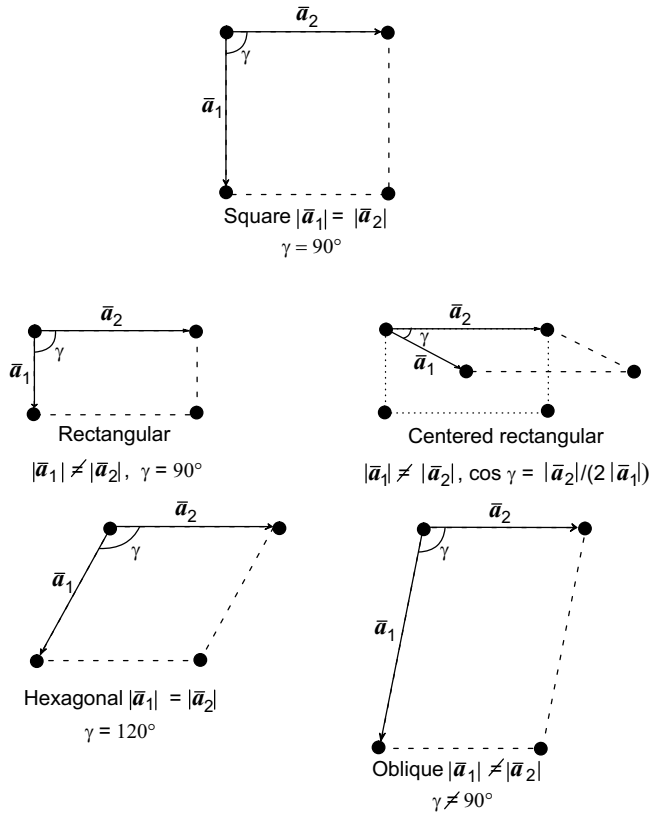

Fig. 1.4. The five two-dimensional Bravais lattices. Besides primitive unit cells (dashed lines) also a non-primitive cell (dotted lines) is shown.

Such a $l = 0$ plane represents a two-dimensional Bravais lattice

$$\boldsymbol{R} = \sum_{i=1}^{2} m_i \bar{\boldsymbol{a}}_i \tag{1.4}$$

with $\bar{\boldsymbol{a}}_1$ and $\bar{\boldsymbol{a}}_2$ as the primitive basis vectors of this lattice and integer numbers m_1 and m_2. The three vectors $\bar{\boldsymbol{a}}_1$, $\bar{\boldsymbol{a}}_2$, $\boldsymbol{n}$ form a right-hand coordinate system. The possible five two-dimensional Bravais lattices of the four planar crystal systems are represented in Fig. 1.4. Apart from the rectangular case, they are primitive (p). In the centered (c) rectangular case additionally the non-primitive cell is also indicated. In practice one often uses the non-primitive lattice for the convenience of description. Sometimes, also non-primitive centered square meshes are used in order to keep a certain orientation of the unit cell.

1.2.2 Oriented Slabs

According to (1.4) all lattice planes in an arbitrary halfspace ($l = 0, -1, -2, ...$) or crystal ($l = 0, \pm 1, \pm 2, ...$) may be described by

$$\boldsymbol{R}_l = \sum_{i=1}^{2} m_i \bar{\boldsymbol{a}}_i + l\bar{\boldsymbol{a}}_3, \tag{1.5}$$

where $\bar{\boldsymbol{a}}_3$ is a vector complementing $\bar{\boldsymbol{a}}_1$ and $\bar{\boldsymbol{a}}_2$ to form a set of (in general) non-primitive lattice vectors $\boldsymbol{a}_1$, $\boldsymbol{a}_2$, $\boldsymbol{a}_3$ of the three-dimensional (3D) bulk lattice of the underlying crystal. The vector $\bar{\boldsymbol{a}}_3$ can be determined from the Diophantine equation $\tilde{\boldsymbol{n}} \cdot \boldsymbol{R}_1 = 1$ with expressions (1.1) and (1.3), as long as the vectors $\bar{\boldsymbol{a}}_1, \bar{\boldsymbol{a}}_2$ satisfy $\tilde{\mathbf{n}} \cdot \boldsymbol{R}_0 = 0$ [1.2]. The choice of $\bar{\boldsymbol{a}}_3$ is not unique, of course, and any vector $\bar{\boldsymbol{a}}_3'$ which differs from $\bar{\boldsymbol{a}}_3$ by a vector within the lattice plane can also be used. We call $\bar{\boldsymbol{a}}_3$ the *stacking vector* because it determines how the chosen lattice planes are stacked in the considered Bravais lattice. For two Bravais lattices Table 1.1 shows a possible choice of the vectors $\bar{\boldsymbol{a}}_1$, $\bar{\boldsymbol{a}}_2$, and $\bar{\boldsymbol{a}}_3$. The vectors $\bar{\boldsymbol{a}}_1$ and $\bar{\boldsymbol{a}}_2$ span the lattice planes shown in Figs. 1.2 and 1.3.

The selection of the three vectors $\bar{\boldsymbol{a}}_1$, $\bar{\boldsymbol{a}}_2$, and $\bar{\boldsymbol{a}}_3$ shows that the primitive cell of a Bravais lattice may be chosen as a parallelepiped with one of its pairs of parallel faces being parallel to a given lattice plane. This implies that such a lattice may be characterized as consisting of parallel lattice planes which are displaced with respect to each other as indicated in Fig. 1.5.

Table 1.1. Possible primitive lattice vectors of a plane and stacking vectors for certain plane orientations in the case of two Bravais lattices. Cubic (a_0) and hexagonal (a, c) lattice constants are used.

3D Bravais lattice	Plane	2D Bravais lattice	$\bar{\boldsymbol{a}}_1$	$\bar{\boldsymbol{a}}_2$	$\bar{\boldsymbol{a}}_3$
fcc	(111)	hexagonal	$\boldsymbol{a}_2 - \boldsymbol{a}_1$	$\boldsymbol{a}_3 - \boldsymbol{a}_2$	$\boldsymbol{a}_1$
$\boldsymbol{a}_1 = \frac{a_0}{2}(0,1,1)$					
$\boldsymbol{a}_2 = \frac{a_0}{2}(1,0,1)$	(110)	p-rectangular	$\boldsymbol{a}_1 - \boldsymbol{a}_2$	$\boldsymbol{a}_1 + \boldsymbol{a}_2 - \boldsymbol{a}_3$	$\boldsymbol{a}_1$
$\boldsymbol{a}_3 = \frac{a_0}{2}(1,1,0)$					
	(100)	p-square	$\boldsymbol{a}_3 - \boldsymbol{a}_2$	$\boldsymbol{a}_1$	$\boldsymbol{a}_2$
hexagonal	(0001)	hexagonal	$\boldsymbol{a}_1$	$\boldsymbol{a}_2$	$\boldsymbol{a}_3$
$\boldsymbol{a}_1 = a(1,0,0)$					
$\boldsymbol{a}_2 = \frac{a}{2}(-1,\sqrt{3},0)$	$(10\bar{1}0)$	p-rectangular	$\boldsymbol{a}_2$	$\boldsymbol{a}_3$	$\boldsymbol{a}_1$
$\boldsymbol{a}_3 = c(0,0,1)$					
	$(11\bar{2}0)$	p-rectangular	$\boldsymbol{a}_2 - \boldsymbol{a}_1$	$\boldsymbol{a}_3$	$\boldsymbol{a}_1$

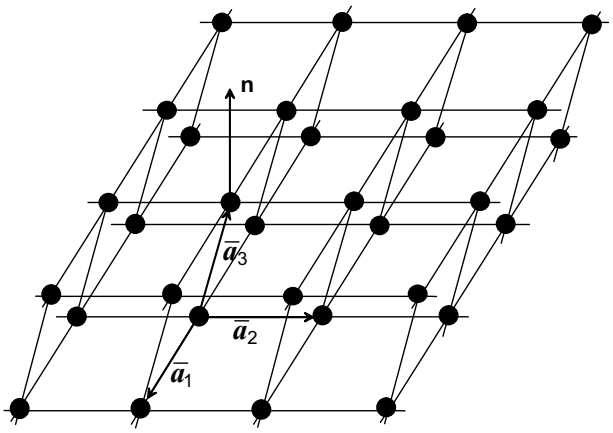

Fig. 1.5. Construction of a 3D Bravais lattice from its lattice planes.

Usually a crystal possesses an atomic basis with S atoms at the positions $\boldsymbol{r}_s$ $(s = 1, ..., S)$ in the unit cell. In correspondence with the lattice planes, atomic planes may be constructed. The lattice plane $\boldsymbol{R}_0$ can be considered to be occupied with atoms of species 1, e.g., at $\boldsymbol{r}_1 = 0$. The next atomic plane, displaced by $\boldsymbol{r}_2$ with respect to the first one, is occupied by atoms of species 2, etc., and the plane displaced by $\boldsymbol{r}_S$ is occupied by atoms of type S. It may happen that two or more atoms of the basis are located at the same plane. In that case an atomic layer (which is later identified with an ideal surface) consists of two or more basis atoms. As a consequence the *polarity* of such a plane can be fixed according to the total charge. In crystals with partially ionic bonds neutral, positively charged or negatively charged atomic planes arise. This allows us to define the polarity of a surface or a corresponding halfspace. For two-atomic crystals with cations and anions, the equal or unequal numbers of these ions in a unit cell spanned by the vectors $\bar{\boldsymbol{a}}_1$ and $\bar{\boldsymbol{a}}_2$ characterize the polarity. The lattice plane $\boldsymbol{R}_0 + \boldsymbol{r}_S$ most distant from $\boldsymbol{R}_0$ completes the construction of a crystal slab which, in the vertical direction, encompasses exactly one primitive unit cell. This slab is called a *primitive crystal slab*. A lattice plane occupied by atoms is referred to as an *atomic layer*. The second primitive crystal slab again begins with a lattice plane occupied by atoms of species 1 and is displaced with respect to the zeroth plane of the first slab by the stacking vector $\bar{\boldsymbol{a}}_3$. A crystal can therefore be thought of as consisting of successive crystal slabs situated one above the other. A pile of several primitive slabs can give a new translational symmetry in the direction of the normal $\boldsymbol{n}$. One calls it an *irreducible crystal slab*. For two-atomic cubic crystals with zinc-blende or diamond structure and lattice constant a_0 such a slab contains three for (111), two for (110), and two for (100) primitive crystal slabs with six for (111), two for (110), and four for (100) atomic layers. The corresponding stacking vectors are

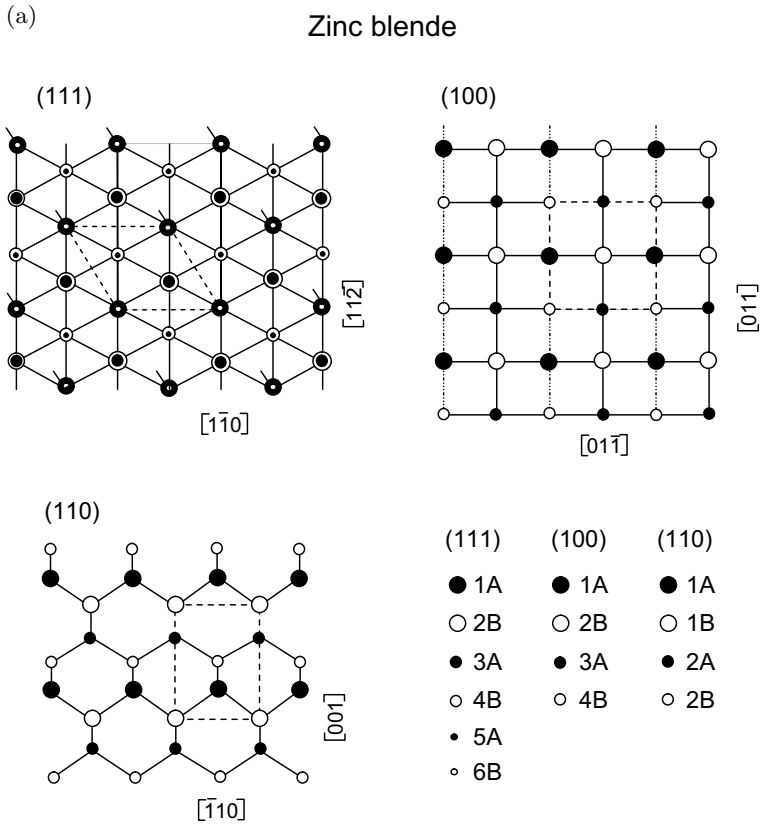

Fig. 1.6. (a) Top view of irreducible crystal slabs with certain orientations $\boldsymbol{n}$ for zinc-blende crystals. The atoms in different layers are indicated by different sizes. Dashed lines indicate a possible 2D unit cell. The size of the filled and open circles indicates the layer beneath the surface. It is related to the layer index $-l$ in the legend. The filling of the circles describes the cation or anion character of the corresponding atom. After [1.2].

$a_0(1,1,1)$, $a_0(1,1,0)$, and $a_0(1,0,0)$. For a two-atomic hexagonal crystal with wurtzite structure such slabs contain four for (0001), three for $(11\bar{2}0)$, and four for $(10\bar{1}0)$ atomic layers. Projections of such irreducible slabs of two-atomic crystals are presented in Fig. 1.6. Crystal examples from two Bravais systems are plotted: fcc with zinc blende (diamond) and rocksalt, hexagonal with wurtzite structure. The corresponding space groups are $F\bar{4}3m$ ($Fd3m$), $Fm3m$, and $P6_3mc$ using the international notation.

The location $\boldsymbol{R}(s,l,m_1,m_2)$ of an individual atom can be specified by the number l of the primitive crystal slab, the number s of the atomic sublattice and the integer coordinates m_1, m_2 of a point in the 2D Bravais lattice as

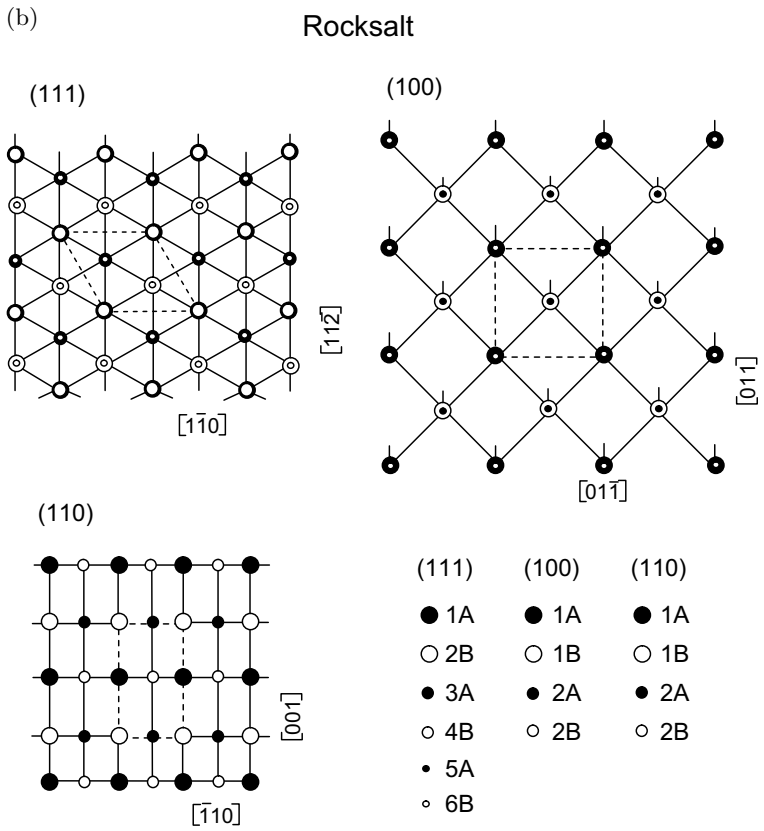

Fig. 1.6. (b) Same as Fig. 1.6a but for rocksalt crystals.

$$\boldsymbol{R}(s, l, m_1, m_2) = \sum_{i=1}^{2} m_i \bar{\boldsymbol{a}}_i + l\bar{\boldsymbol{a}}_3 + \boldsymbol{r}_s. \tag{1.6}$$

The complete set of atomic sites in an infinite 3D crystal can be obtained by assigning all possible integer values from $-\infty$ to $+\infty$ for l, m_1, m_2 and all possible values $s = 1, ..., S$. The normal direction $\boldsymbol{n}$, upon which the construction of the lattice planes is based, is without influence on the sites. Any choice of $\boldsymbol{n}$ yields the same crystal.

1.2.3 Ideal Surfaces. Planar Point Groups

The above representation (1.6) of an infinite crystal can immediately be employed in describing a crystal with an ideal surface and normal $\boldsymbol{n}$, i.e., a halfspace. Such a system may be generated from an infinite crystal by removing all atomic layers above the surface and retaining those below. The

(c)

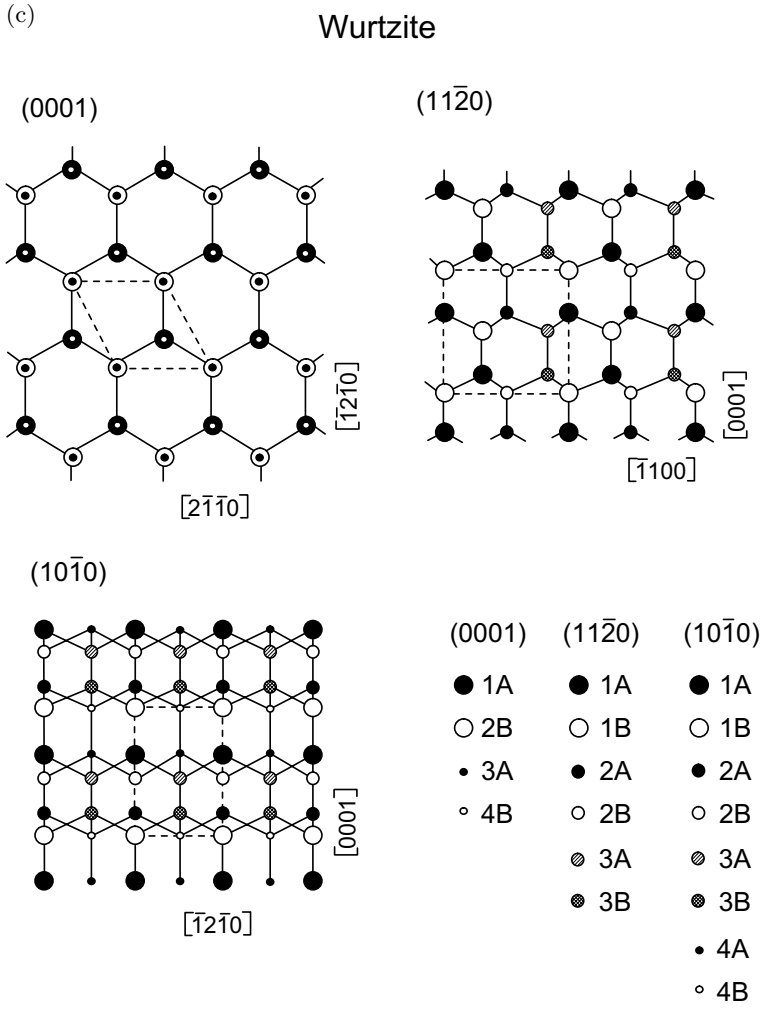

Fig. 1.6. (c) Same as Fig. 1.6a but for wurtzite crystals.

remaining uppermost atomic layer represents the surface or, at least, the uppermost atomic layer of the surface region of the resulting halfspace. How many atomic layers are counted to belong to the surface region depends on the method used to investigate the system, e.g., on the penetration depths of the exciting and/or detected particles.

In a first approach one may assume that the atoms in the uppermost atomic layers, in particular in the topmost layer, keep the atomic positions of the infinite crystal. Such a configuration is usually termed an *ideal surface*. The atoms of a crystal having an ideal surface are thus located at the positions

$\boldsymbol{R}(s, l, m_1, m_2)$ given by (1.6). However, only sites below the surface plane are occupied. These obey the relation

$$\tilde{\boldsymbol{n}} \cdot \boldsymbol{R}(s, l, m_1, m_2) = l + \tilde{\boldsymbol{n}} \cdot \boldsymbol{r}_s \leq 0 \tag{1.7}$$

with $\tilde{\boldsymbol{n}}$ given in expression (1.1). The *surface* or first atomic layer is obtained if the left-hand side of this relation is taken to be zero. A possible solution of (1.7) is $l = 0$ and $\boldsymbol{r}_{s_0} = 0$, so long as the site of one atom s_0 of the atomic basis is identified with a Bravais lattice point. Thus, the first atomic layer corresponds to the particular lattice plane perpendicular to the normal $\boldsymbol{n}$ which goes through zero and whose lattice points are occupied by basis atoms of species s_0. There may be other vectors $\boldsymbol{r}_s$ beside $\boldsymbol{r}_{s_0}$ which, although not being zero themselves, have a zero projection $\boldsymbol{n} \cdot \boldsymbol{r}_s$. Then the basis atoms of this species s are also located in the first atomic layer. They are displaced with respect to the atoms of species s_0 by a vector $\boldsymbol{r}_s$ parallel to the surface. Such multiple-species occupancy of an atomic layer occurs, for instance, in the case of (110) surfaces of zinc-blende-type crystals. In this case, two atoms – a cation and an anion – occur in each primitive unit cell of such a 2D crystal. The (110) surface forms a non-polar face because of charge neutrality, which is one of the reasons why the (110) plane represents the cleavage face of zinc-blende crystals.

The resulting halfspace with an ideal, bulk-terminated surface (or even a real surface as discussed below) exhibits not only a 2D periodicity or, more precisely, a 2D translational symmetry with the primitive basis vectors $\bar{\boldsymbol{a}}_1$ and $\bar{\boldsymbol{a}}_2$ but also a point symmetry. As a consequence of the translational symmetry according to the 2D Bravais lattice points $\boldsymbol{R}$ (1.4), physically equivalent space points can be related by

$$\begin{aligned} \boldsymbol{x}' &= \{\varepsilon|\boldsymbol{R}\}\,\boldsymbol{x} \\ &= \hat{\varepsilon}\boldsymbol{x} + \boldsymbol{R} = \boldsymbol{x} + \boldsymbol{R}, \end{aligned} \tag{1.8}$$

where $\hat{\varepsilon}$ denotes the transformation matrix characterizing the element ε. Such points are displaced against each other by a Bravais lattice vector $\boldsymbol{R}$. No rotation or reflection is involved. This is indicated by the unit element ε and the unit matrix $\hat{\varepsilon}$, respectively. All elements which belong to a certain *translational group* are abbreviated by $\{\varepsilon|\boldsymbol{R}\}$. However, in addition there can be point group operations $\{\alpha|0\}$ which also relate physically equivalent space points $\boldsymbol{x}'$ and $\boldsymbol{x}$. The point symmetry elements α are necessarily rotations about axes which are parallel to the normal $\boldsymbol{n}$, and reflections at lines within the surface or cell planes perpendicular to $\boldsymbol{n}$. Only $n = 1, 2, 3, 4$, or 6-fold rotation axes perpendicular to the surface may occur. Correspondingly, the symbol δ_n^m signifies a rotation around the surface normal direction by the angle $(360\ m/n)^\circ$ with $m = 0, 1, ..., n-1$. The mirror planes are also normal to the surface. Inversion centers, mirror planes and rotation axes parallel to the surface are not allowed, since they refer to points outside the surface. The possible reflection lines m_x, m_y, m_1, m_2, m_d, m_1', m_2', and m_d' are specified in Fig. 1.7.

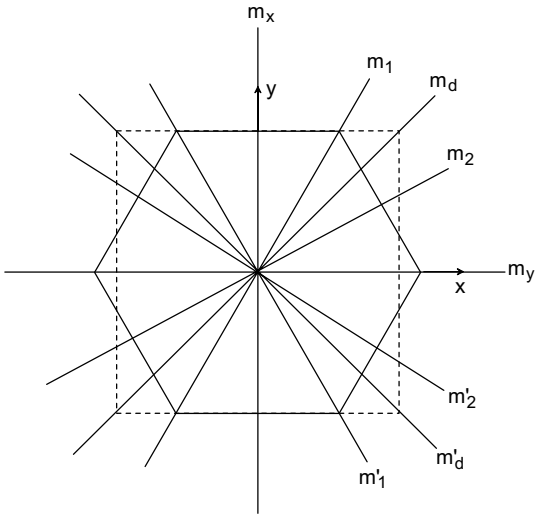

Fig. 1.7. Denotation of reflection lines.

By combining the limited number of allowed symmetry operations, one obtains 10 different *plane point groups*. In the international system (Schoenflies system) they are denoted by either n (C_n) or nm, nmm (C_{nv}). The numeral $n = 1, 2, 3, 4, 6$ denotes rotations by $\frac{2\pi}{n}$ and the symbol m refers to reflections in a mirror plane. The third symbol m indicates that a combination of the preceding two operations generates a new mirror plane. The 10 point groups are 1 (C_1), 2 (C_2), m (C_{1v}), $2mm$ (C_{2v}), 3 (C_3), $3m$ (C_{3v}), 4 (C_4), $4mm$ (C_{4v}), 6 (C_6), $6mm$ (C_{6v}). They are geometrically represented in Fig. 1.8.

The plane Bravais lattices presented in Fig. 1.4 also possess point symmetries. However, the possible multiplicities of a rotation symmetry axis of plane lattices are restricted to $n = 2, 4$ and 6. A lattice which only contains a 2-fold symmetry axis is either an oblique lattice or a rectangular one (independent of the p- or c-character). The point groups of these lattices are 2 (C_2) and $2mm$ (C_{2v}), respectively. Quadratic lattices with a 4-fold symmetry axis possess four reflection lines which are rotated through 45° with respect to each other. The point group of such a lattice is therefore $4mm$ (C_{4v}). Hexagonal lattices with a 6-fold axis have six reflection lines which meet at an angle of 30°. In this case the point group is $6mm$ (C_{6v}). Summarizing, there are thus four different plane *crystal systems* – the oblique with the *holohedral point group* 2, the rectangular with the *holohedral point group* $2mm$, the quadratic with the *holohedral point group* $4mm$, and the hexagonal with the *holohedral point group* $6mm$. These crystal systems contain five 2D Bravais lattices (cf. Fig. 1.4).

The low-Miller-index surfaces of face-centered cubic and body-centered cubic metal crystals exhibit such high point-group symmetries because of their structural simplicity. As indicated in Fig. 1.2, these surfaces tend to

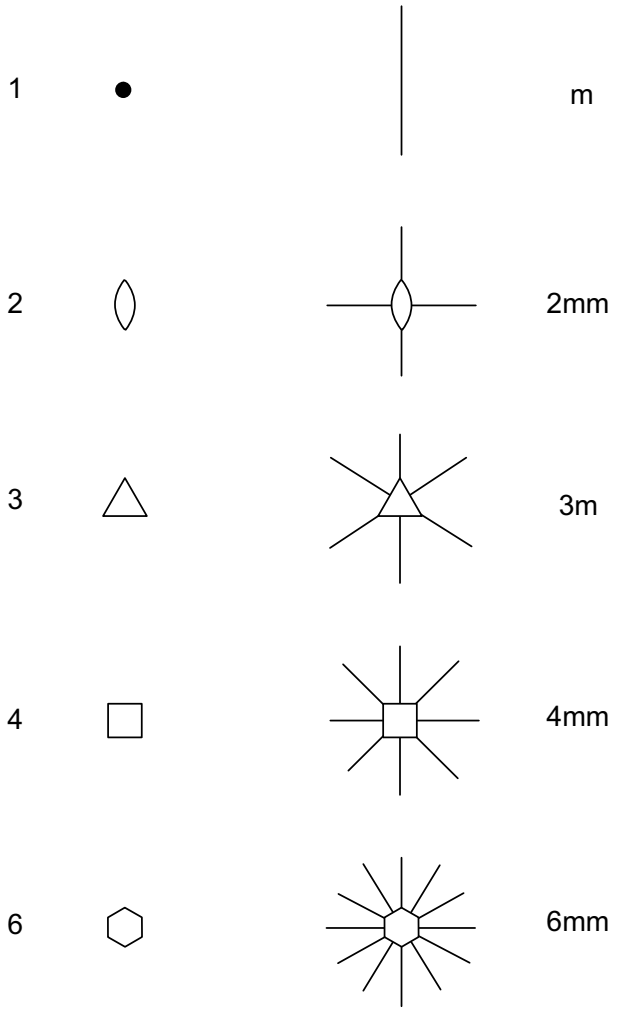

Fig. 1.8. Schematic representation of the 10 plane point groups.

have the highest degree of symmetry and the smallest unit cells. Examples are fcc(111), fcc(110), and fcc(100), which have threefold, twofold, and fourfold rotational symmetry, respectively. Other examples are bcc(111), bcc(110), and bcc(100), which have threefold, twofold, and fourfold rotational symmetry, respectively. Isolated (111) planes even possess a higher rotational (sixfold) symmetry. Of course, all these surfaces also have mirror planes in addition to the rotation axes.

1.2.4 Real Surfaces: Reconstruction and Relaxation

The 2D translational symmetries of ideal surfaces and halfspaces with bulk atomic positions are characterized by the primitive Bravais vectors $\bar{\boldsymbol{a}}_1$ and $\bar{\boldsymbol{a}}_2$. In addition to point and line defects (cf. Fig. 1.1), on a real surface of a crystal there are other reasons that the assumption of an ideal surface is not valid in general. Such a picture does not fully account for the bonding behavior of the atoms in a crystal. Since the forces acting on atoms situated beneath an atomic plane in an infinite crystal are partially due to the atoms located above the plane, one can, in general, expect that the forces acting on atoms in a crystal with a surface should differ from those acting in an infinite crystal. The deviation from the infinite case, however, diminishes with increasing distance of the atoms from the surface. One can thus assume that the forces acting on, and hence the position of, atoms deep inside the crystal bulk are, to a good approximation, the same as those in an infinite crystal. This is, however, not true for atoms situated near the surface. The forces acting on them are appreciably different, resulting in displacements $\delta\boldsymbol{R}(s,l,m_1,m_2)$ of atomic positions $\boldsymbol{R}(s,l,m_1,m_2)$ (1.6) with respect to those of the infinite crystal. Consequently, the equilibrium conditions for surface atoms are modified with respect to the infinite crystal. One expects altered atomic positions

$$\boldsymbol{R}'(s,l,m_1,m_2) = \boldsymbol{R}(s,l,m_1,m_2) + \delta\boldsymbol{R}(s,l,m_1,m_2), \tag{1.9}$$

with

$$\delta\boldsymbol{R}(s,l,m_1,m_2) \to 0 \quad \text{for} \quad l \to -\infty, \tag{1.10}$$

and a surface atomic structure that usually does not agree with that of the bulk. Thus a surface is not merely a truncation of the bulk of a crystal.

The distortion of the ideal bulk-like atomic configuration due to the existence of a surface (more precisely, the non-existence of formerly neighboring atoms in the vacuum) depends on the bonding behavior of the material considered. In tetrahedrally bonded semiconductors, such as diamond, Si, Ge, GaAs, InP, GaN, etc., strong directional bonds are present. The breaking of bonds due to the generation of the surface is expected to have dramatic effects. Systems with dangling bonds should be in general unstable, since rebonding usually lowers the total energy of the halfspace. Sometimes, this process is accompanied by bringing surface atoms closer together. One of these mechanisms resulting in pairs of surface atoms is schematically indicated in Fig. 1.9a. However, such a rearrangement can also yield rough surface layers, the stoichiometry of which is changed with respect to the ideal surface (see Fig. 1.9b). In both cases, the 2D Bravais lattice of the surface is changed. Such perturbations destroying the translational symmetry of the fictitious ideal surface are known as *surface reconstruction*.

There are general arguments for such symmetry-breaking atomic rearrangements. One is based on the impossibility of degenerate ground states

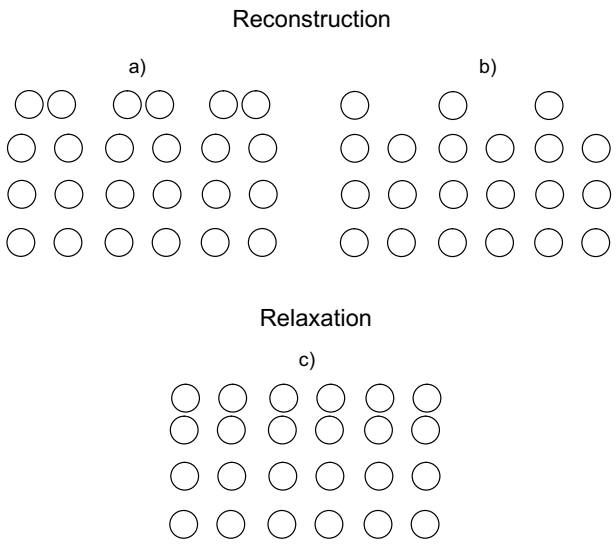

Fig. 1.9. Schematic illustrations of atomic rearrangements in the surface region. (a) Pairing reconstruction; (b) missing row reconstruction; and (c) relaxation of the uppermost atomic layer.

of the system. Such a degeneracy may occur, for instance, for (111) surfaces of diamond-structure crystals. In their case, on average there is only one electron for each dangling-bond orbital parallel to the [111] surface normal, although each orbital can accomodate two electrons of opposite spins. The system ground state can thus be realized in numerous ways by placing two electrons in two orbitals, two in one or an equal distribution over the dangling bonds. However, the arrangement of these orbitals may differ. According to the well-known *Jahn–Teller theorem* spontaneous symmetry breaking will occur [1.3]. The degeneracy is lifted. In the discussed (111) case this implies Jahn–Teller displacements of the surface atoms which destroy their equivalence. One may at least expect a so-called 2×1 reconstruction, in a sense that is explained below.

In simple metals, instead one has a gas of quite delocalized electrons and chemical bonds which are far less directional than in semiconductors. Consequently, there are no preferred directions in the displacements of atoms with the exception of that parallel to the surface normal vector itself. One thus expects a displacement mainly of the first-layer atoms in a vertical direction with respect to the surface as indicated in Fig. 1.9c. The 2D Bravais lattice and, hence, the 2D translational symmetry remains unchanged. Such a translational-symmetry-conserving change of the atomic structure is called *surface relaxation*. A special argument for simple metals is based on the local charge neutrality. In the bulk the nearly free electrons are delocalized between the cores making an electrically neutral object. On a surface (see Fig. 1.10a),

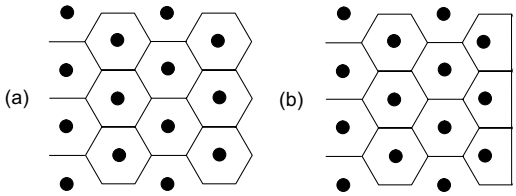

Fig. 1.10. Schematic representation of a metal surface by cores (dots) and Wigner–Seitz cells (hexagons) before (a) and after (b) the surface relaxation. Deformations of hexagons indicate the redistribution of the electron density accompanying its smearing out at the surface and the inward displacements of the cores.

this picture would lead to a rapidly varying electron density at the surface, according to the arrangement of the bulk atomic sites. As indicated schematically in Fig. 1.10b the surface electronic charge tends to smooth out, which is only possible by vertical displacements of the ion cores. Simultaneously, the electrostatic repulsion of first- and second-layer ions is reduced, which results in the inward direction of the relaxation (contraction). The effect is observed for many low-index metal surfaces.

Reconstructions, for instance that of the type indicated in Fig. 1.9b, can also occur at metal surfaces. However, the relaxation is not restricted to metals but can also occur for surfaces of nonmetals. The clean cleaved GaAs(110) surface is one well-known example in this respect [1.4]. Due to the electrostatic neutrality of the surface unit cell with one cation and one anion (cf. Fig. 1.6), two dangling bonds and two electrons are available. Consequently, there is no need for Jahn–Teller displacements. Instead, opposite vertical displacements, i.e., a surface buckling accompanied by an electron transfer between the dangling bonds, stabilize the surface translational symmetry known from the truncated bulk.

Besides the arguments of the saturation of dangling bonds or smoothness of electron distributions, another argument is related to the reduction of the electrostatic energy of systems with partially ionic bonds. Due to their Coulomb character, the electrostatic interaction of ions is of long-range nature and does not show a directional dependence. Since the only defined direction in the system is still the surface normal, again a tendency to a special type of relaxation occurs. One example for a class of corresponding crystals concerns $A_{IV}B_{VI}$ semiconductors with partially ionic bonds and rocksalt structure. Two different types of surfaces are possible in these crystals, a polar type with exclusively A or B atoms, and a non-polar type with both A and B atoms in the surface (see Fig. 1.6). In the case of the non-polar (100) surfaces one expects from considerations of the Madelung energy vertical displacements of the surface atoms but none parallel to the surface plane. Both sublattices, A and B, should relax inward but to different degrees, because of their different ion sizes. This results in a so-called *rumpling* of the surface [1.5].

1.2.5 Superlattices at Surfaces

In accordance with the above discussions, the atomic displacements $\delta\boldsymbol{R}(s, l, m_1, m_2)$ in expression (1.9) may be divided into two classes with regard to their effect on the translational symmetry of the surface. If the translational symmetry is not affected, the displacements represent a relaxation of the surface (see Fig. 1.11a). Then $\delta\boldsymbol{R}(s, l, m_1, m_2) = \delta\boldsymbol{r}_{sl}$ for all m_1, m_2. Only the vectors $\boldsymbol{r}_{sl}$ of the atomic basis in the halfspace belonging to the 2D Bravais lattice are altered. In the case of surface reconstruction (see Fig. 1.11b) equivalent atoms in different unit cells are not all displaced in the same manner, i.e., $\delta\boldsymbol{R}(s, l, m_1, m_2)$ depends on m_1 and m_2. Both the atomic basis and the Bravais lattice are changed.

In the case of a reconstructed surface a new 2D Bravais lattice with primitive basis vectors $\bar{\bar{\boldsymbol{a}}}_1$ and $\bar{\bar{\boldsymbol{a}}}_2$ occurs. In this situation a periodicity is present in the topmost atomic layers which is different from the corresponding 2D translational symmetry with $\bar{\boldsymbol{a}}_1$ and $\bar{\boldsymbol{a}}_2$ in bulk-like layers deep below the surface. In other words, a surface lattice, called a *superlattice*, is superimposed on the substrate lattice which exhibits the basic periodicity. Consequently, two translational groups T_s (characterizing the uppermost surface layers by $\bar{\bar{\boldsymbol{a}}}_1$, $\bar{\bar{\boldsymbol{a}}}_2$) and T_b (characterizing bulk-like layers by $\bar{\boldsymbol{a}}_1$, $\bar{\boldsymbol{a}}_2$) have to be discussed. The translations which transform the crystal with surface (the halfspace) into itself must belong to both groups of translations, T_s and T_b. The translational group T of the whole crystal with surface is thus the intersection

$$T = T_\mathrm{s} \cap T_\mathrm{b}. \tag{1.11}$$

Alternatively, one can say that T is the largest common subgroup of both groups T_s and T_b. There are two possiblities. Either T only consists of the identity translation, which means that the lattices defined by T_s and T_b are *non-commensurate*, or T contains more elements than just the identity, which means that the surface (T_s) and bulk (T_b) are *commensurate*. In the first case, the crystal with surface does not possess any lattice-translational symmetry. Realizations of non-commensurate surfaces are more likely in the case of adsorption. In the second case, the lattice associated with T is called a *co-*

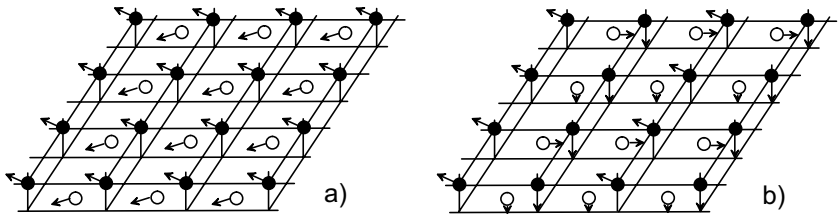

Fig. 1.11. Examples for surface relaxation (a) and surface reconstruction (b) influencing the first and second atomic layers. A 2×2 reconstruction is shown in (b).

incidence lattice. If, in particular, T_s is a subgroup of T_b, then T is equal to T_s, i.e., the coincidence lattice is identical with the lattice of the surface. If T_s is not a subgroup of T_b, then T cannot be equal to T_s and is necessarily a proper subgroup of T_s, i.e., it is smaller than T_s.

In general, the primitive vectors $\bar{\bar{\boldsymbol{a}}}_1$, $\bar{\bar{\boldsymbol{a}}}_2$ of the surface Bravais lattice and those $\bar{\boldsymbol{a}}_1$, $\bar{\boldsymbol{a}}_2$ of the corresponding bulk-like layers are related by

$$\bar{\bar{\boldsymbol{a}}}_i = \sum_{j=1}^{2} m_{ij} \bar{\boldsymbol{a}}_j, \tag{1.12}$$

i.e., by a 2×2 matrix $\hat{M}$ with

$$\hat{M} = \begin{pmatrix} m_{11} & m_{12} \\ m_{21} & m_{22} \end{pmatrix}. \tag{1.13}$$

This matrix can be used to denote the surface superlattice structure. It results in the so-called matrix notation. The matrix also allows a convenient classification of the relation of two 2D lattices. There are three pertinent cases:

i. When all matrix elements m_{ij} are integers, the lattices of the surface region and the bulk substrate are simply related. The surface lattice is called a simple superlattice.
ii. When all matrix elements m_{ij} are rational numbers, the two lattices are rationally related. The surface is said to have a coincidence structure, and the superstructure is referred to as commensurate.
iii. When at least one matrix element m_{ij} is an irrational number, the two lattices are irrationally related, and the superstructure is termed incoherent or incommensurate.

In the first and second cases, the combined surface layer and bulk substrate is characterized also by a Bravais lattice, and the surface layer is in complete or partial coincidence with the substrate. The three cases (i), (ii), and (iii) can more easily be characterized by the determinant of $\hat{M}$, $\det \hat{M}$, where $\det \hat{M}$ is an integer, rational, or irrational number. Geometrically $\det \hat{M}$ relates the areas of the primitive unit cells spanned by the vectors $\bar{\bar{\boldsymbol{a}}}_1$, $\bar{\bar{\boldsymbol{a}}}_2$ and $\bar{\boldsymbol{a}}_1$, $\bar{\boldsymbol{a}}_2$. In any case the matrix $\hat{M}$ can be used to characterize a reconstructed surface. The corresponding notation is called *matrix notation*.

1.2.6 Wood Notation

As an alternative to the matrix notation, the more transparent *Wood notation* [1.6] is used in many cases as a labeling scheme for the reconstructed surface and the occurring superstructure. The first step is the characterization of the (hkl) crystallographic orientation of the substrate surface (more precisely, the plane) with the chemical composition S by $S(hkl)$. There is a simple notation

for the reconstruction-induced superstructures in terms of the ratios of the lengths of the primitive lattice vectors of the two 2D Bravais lattices under consideration. Such a surface is characterized by

$$S(hkl)\kappa \left(\frac{|\bar{\bar{\boldsymbol{a}}}_1|}{|\bar{\boldsymbol{a}}_1|} \times \frac{|\bar{\bar{\boldsymbol{a}}}_2|}{|\bar{\boldsymbol{a}}_2|} \right) R\varphi^\circ. \tag{1.14}$$

In the notation (1.14), κ is either 'p' (for primitive) or 'c' (for centered) according to the way in which the unit cell of the surface Bravais lattice is defined. When the letter 'p' is dropped, the primitive notation is understood implicitly. The quantity $(m{\times}n) = (|\bar{\bar{\boldsymbol{a}}}_1|/|\bar{\boldsymbol{a}}_1|{\times}|\bar{\bar{\boldsymbol{a}}}_2|/|\bar{\boldsymbol{a}}_2|)$ indicates the ratios of the magnitudes of the (usually) primitive basis vectors of the surface lattice and the bulk beneath. One speaks about an $(m \times n)$ reconstruction. The symbol $R\varphi^\circ$ includes the possibility of a rotation (R) of the unit cell of the overlayer by φ degrees with respect to the unit cell of the substrate, i.e., the angle between $\bar{\bar{\boldsymbol{a}}}_1$ and $\bar{\boldsymbol{a}}_1$. If φ is zero, then $R\varphi^\circ$ is omitted from (1.14). Consequently, typical denotations could be

$$S(hkl)m \times n, \quad S(hkl)c(m \times n), \text{ and } \quad S(hkl)(m \times n)R\varphi^\circ. \tag{1.15}$$

Examples are plotted in Fig. 1.12. For a couple of examples of reconstructions the relation between the Wood notation (1.14) and the matrix notation (1.13) is given in Table 1.2 [1.7].

Several additional remarks are necessary. First, sometimes the Wood notation is not unequivocal. The lattice vectors $\bar{\bar{\boldsymbol{a}}}_1 = m\bar{\boldsymbol{a}}_1$ and $\bar{\bar{\boldsymbol{a}}}_2 = n\bar{\boldsymbol{a}}_2$ are not necessarily primitive as originally assumed in the notation (1.14), and in addition to primitive (p) reconstructed surface lattices, also centered (c) ones

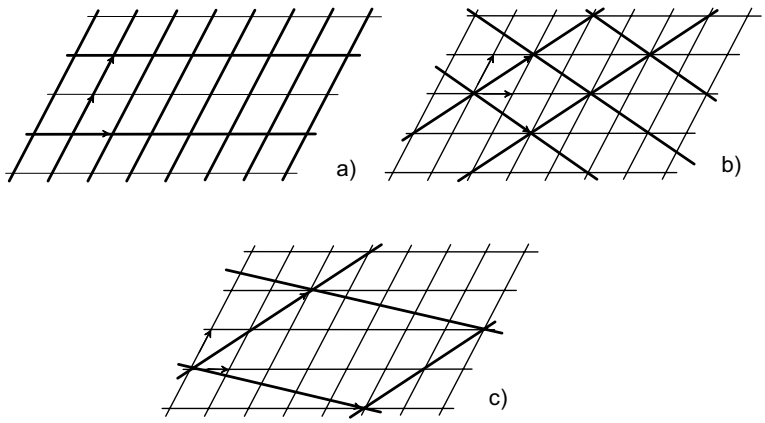

Fig. 1.12. Three different types of surface reconstructions. (a) 1×2, (b) $(\sqrt{3}{\times}\sqrt{3})R30^\circ$, and (c) general case. The Wood notation does not apply in this case; however the matrix notation does with $m_{11} = 5$, $m_{12} = -1$, $m_{21} = 2$, $m_{22} = 2$.

Table 1.2. Wood and matrix notation of reconstructed surfaces of cubic and hexagonal crystals [1.7].

	Reconstruction	
Ideal surface	Wood notation	Matrix notation
	$p(1\times1)\hat{=}1\times1$	$\begin{pmatrix}1&0\\0&1\end{pmatrix}$
fcc(100),	$p(2\times1)\hat{=}2\times1$	$\begin{pmatrix}2&0\\0&1\end{pmatrix}$
bcc(100),	$p(1\times2)\hat{=}1\times2$	$\begin{pmatrix}1&0\\0&2\end{pmatrix}$
diamond(100),	$c(2\times2)\hat{=}(\sqrt{2}\times\sqrt{2})R45^\circ$	$\begin{pmatrix}1&\bar{1}\\1&1\end{pmatrix}$
zinc blende(100)	$p(2\times2)\hat{=}2\times2$	$\begin{pmatrix}2&0\\0&2\end{pmatrix}$
	$(2\sqrt{2}\times\sqrt{2})R45^\circ$	$\begin{pmatrix}2&2\\\bar{1}&1\end{pmatrix}$
	$c(4\times2)$	$\begin{pmatrix}2&\bar{1}\\0&2\end{pmatrix}$
	$p(1\times1)\hat{=}1\times1$	$\begin{pmatrix}1&0\\0&1\end{pmatrix}$
fcc(111),	$p(2\times1)\hat{=}c(2\times2)\hat{=}2\times1$	$\begin{pmatrix}2&0\\0&1\end{pmatrix}$
hcp(0001),	$p(2\times2)\hat{=}2\times2$	$\begin{pmatrix}2&0\\0&2\end{pmatrix}$
diamond(111),	$(\sqrt{3}\times\sqrt{3})R30^\circ$	$\begin{pmatrix}1&1\\\bar{1}&2\end{pmatrix}$
zinc blende(111),	$c(4\times2)$	$\begin{pmatrix}2&\bar{1}\\0&2\end{pmatrix}$
graphite(0001)	$(\sqrt{7}\times\sqrt{7})R\arctan(\sqrt{3}/5)$	$\begin{pmatrix}2&1\\\bar{1}&3\end{pmatrix}$
	$p(1\times1)\hat{=}1\times1$	$\begin{pmatrix}1&0\\0&1\end{pmatrix}$
fcc(110),	$p(2\times1)\hat{=}2\times1$	$\begin{pmatrix}2&0\\0&1\end{pmatrix}$
diamond(110),	$p(1\times2)\hat{=}1\times2$	$\begin{pmatrix}1&0\\0&2\end{pmatrix}$
zinc blende(110)	$c(2\times2)$	$\begin{pmatrix}1&\bar{1}\\1&1\end{pmatrix}$
	$p(1\times1)\hat{=}1\times1$	$\begin{pmatrix}1&0\\0&1\end{pmatrix}$
bcc(110)	$p(2\times1)\hat{=}2\times1$	$\begin{pmatrix}2&0\\0&1\end{pmatrix}$
	$p(2\times2)\hat{=}2\times2$	$\begin{pmatrix}2&0\\0&2\end{pmatrix}$

are possible. This can only take place, however, for rectangular surface lattices. Thus, the modified notation applies only to this case, although it is also sometimes used (formally incorrectly) for square lattices. In the rectangular case the notation $c(n\times m)$ describes a type of reconstruction which is usually not covered by one of the notations $n'\times m'$ or $(n''\times m'')R\varphi^\circ$. For square reconstructed lattices the $c(n\times m)$ notation is just a simpler description of a reconstruction of type $(n'\times m')R45^\circ$. One example is shown in Fig. 1.13.

Second, another problem is related to the fact that one and the same reconstruction may be defined in different ways. The problem is a consequence of the high point symmetry of the crystal with an ideal surface. If the latter has a square lattice and one of the two point symmetry groups $4mm$ or 4, the directions of the two primitive lattice vectors are symmetrically equivalent. A surface reconstruction which increases the surface unit cell in the

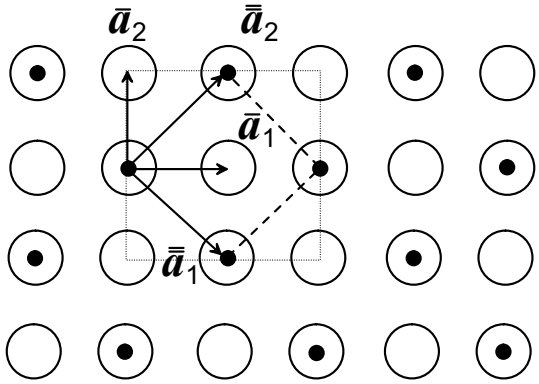

Fig. 1.13. A surface superstructure with the possible denotations $c(2\times2)$ and $(\sqrt{2}\times\sqrt{2})R45^\circ$.

direction of $\bar{\boldsymbol{a}}_1$ by a factor n and in the direction of $\bar{\boldsymbol{a}}_2$ by a factor m, is equivalent to an $m \times n$ reconstruction. An example is given in Fig. 1.14. An analogous statement holds for an ideal surface, having a hexagonal lattice and one of the point groups $6mm$, 6, $3m$, or 3. In this case, three symmetrically equivalent directions exist (see Fig. 1.14). If there is no physical reason which makes one of the geometrically different but symmetrically equivalent reconstructions more likely than another, they will take place simultaneously in different regions of the surface. As a result domains can be formed of otherwise identical, but differently oriented, reconstructed unit cells. Due to the domain structure, the overall translational symmetry of the surface is destroyed. Structural imperfections of a more local nature occur where the boundaries of such domains meet. In the case of the Si(111) surface, the 2×1 unit meshes may occur in one, two or all three $\langle 211 \rangle$ directions, depending on the cleavage conditions [1.8].

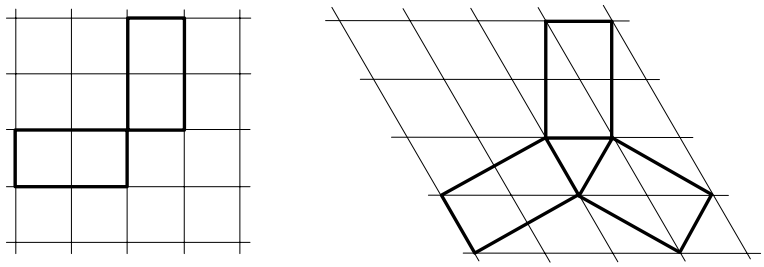

Fig. 1.14. Symmetrically equivalent 2×1 reconstructions of square and hexagonal ideal lattices.

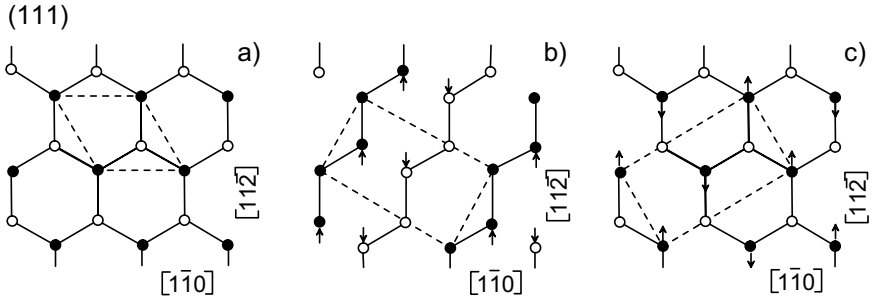

Fig. 1.15. Two different 2×1 reconstructions of the (111) surface of diamond-structure crystals. (a) ideal surface; (b) 2×1 reconstructed surface due to chain formation; and (c) 2×1 reconstructed surface due to an inequivalent buckling of surface atoms. Dots: nominal first-layer atoms; circles: nominal second-layer atoms.

Third, a certain reconstruction denoted by an expression of the type (1.14) can be realized by different atomic configurations. This is demonstrated in Fig. 1.15 for different arrangements of first- and second-layer atoms of a diamond-like material (111) surface. The easiest way to reconstruct the ideal surface (Fig. 1.15a) is by buckling the first-layer atoms (Fig. 1.15c). The dangling bonds parallel to [111] become inequivalent. The accompanying different filling with electrons supports the tendency to an inert surface. However, the dangling bonds can also be rebonded if they occur at atoms which are first-nearest neighbors (from the bulk point of view). The surface atoms may be arranged in the form of chains lying next to each other (see a possible example in Fig. 1.15b). All atoms of a chain are coupled together by π-bonds of parallel dangling orbitals. The generation of dangling bonds at the formerly second-layer atoms include remarkable changes of the bonding topology beneath. The atoms in bulk crystals of the diamond structure are bonded in sixfold rings. In a π-bonded chain model [1.9], however, fivefold and sevenfold rings are formed.

Fourth, the Wood notation can also be used for surface overlayer structures due to adsorbates. A periodic arrangement of adatoms or adsorbed molecules also gives rise to a superstructure, which can be classified according to expression (1.14). However, one usually adds a term $-\eta A$ to the Wood notation. The chemical stoichiometry of the atomic or molecular overlayer is given by A, and η is the number of adspecies in the overlayer unit cell. For example, CO adsorbed molecularly on the Ni(100) surface at a fractional surface coverage of one half forms an overlayer shown by the dots in Fig. 1.13. According to expression (1.14), in this case the surface denotation becomes Ni(100)$c(2\times2)$-CO or Ni(100)$(\sqrt{2}\times\sqrt{2})R45°$-CO.

1.2.7 Symmetry Classification

In the commensurate case all the reconstructed surfaces with the underlying bulk halfspaces possess a translational symmetry characterized by the four Bravais classes with group elements $\{\varepsilon|\boldsymbol{R}\}$. The corresponding 2D Bravais lattice transforms according to a certain planar point group (see Fig. 1.8), the so-called holohedral point group, with elements $\{\alpha|0\}$. The 2D crystal, the atoms in the surface and the bulk below, transform according to a subgroup, its point group. The combination of the translational and point group symmetries gives the space group. There are 17 planar space groups. Lattices with a corresponding symmetry are shown in Fig. 1.16.

It is evident that each of the 10 point groups of equivalent directions combined with the corresponding associated lattice gives rise directly to a so-called symmorphic space group with elements $\{\alpha|\boldsymbol{R}\}$. The space groups $p1$, $p211$, $p1m1$, $p2mm$, $p4$, $p4mm$, $p3$, $p3m1$, $p6$, and $p6mm$ originate in this manner. Since the point groups of the rectangular crystal system are each associated with two Bravais lattices, primitive or centered, we find two further space groups, $c1m1$ and $c2mm$. In the case of the point group $3m$ there exist two different possibilities of positioning two reflection lines relative to the hexagonal lattice vectors, either through the vertices of the equilateral hexagon of the Wigner–Seitz cell as assumed in the case of $p3m1$, or such that they bisect its edges. In the latter case one has, as the thirteenth space group, the group $p31m$. The point group remains unchanged if in its space group a glide reflection line is substituted for an ordinary reflection line. One must therefore examine the 13 space groups already established to determine whether the substitution of a reflection line m by a glide reflection line g (i.e., a reflection in m in conjunction with a translation $\boldsymbol{\tau}$ by half of the shortest lattice vector parallel to m) leads to a new space group. One easily finds that this is not the case for the hexagonal crystal system. In the quadratic crystal system it is possible to substitute a system of glide reflection lines for one but not both of the non-equivalent reflection line systems. This yields the additional space group $p4gm$. The remaining space groups $p1g1$ (from $p1m1$) and $p2mg$, $p2gg$ (from $p2mm$) occur in 2D crystals with a primitive rectangular Bravais lattice. They contain elements of the form $\{\alpha|\boldsymbol{R}+\boldsymbol{\tau}\}$ with $\boldsymbol{\tau}$ as a fractional lattice translation. The centered rectangular and oblique crystal systems do not give rise to additional space groups. Consequently, four of the 17 2D space groups involve glide reflections, i.e., they are nonsymmorphic groups.

In Table 1.3 we summarize the symmetry classification of 2D crystals. The international notation is used. Despite the fact that the atomic basis is extended parallel to the negative surface normal direction, we use a plane rectangular coordinate system with unit vectors $\boldsymbol{e}_x$, $\boldsymbol{e}_y$. The origin of the coordinate system is positioned on the rotation axis, if one exists. The primitive basis vectors of the 2D Bravais lattice are $\bar{\boldsymbol{a}}_1$, $\bar{\boldsymbol{a}}_2$. The second bar indicat-

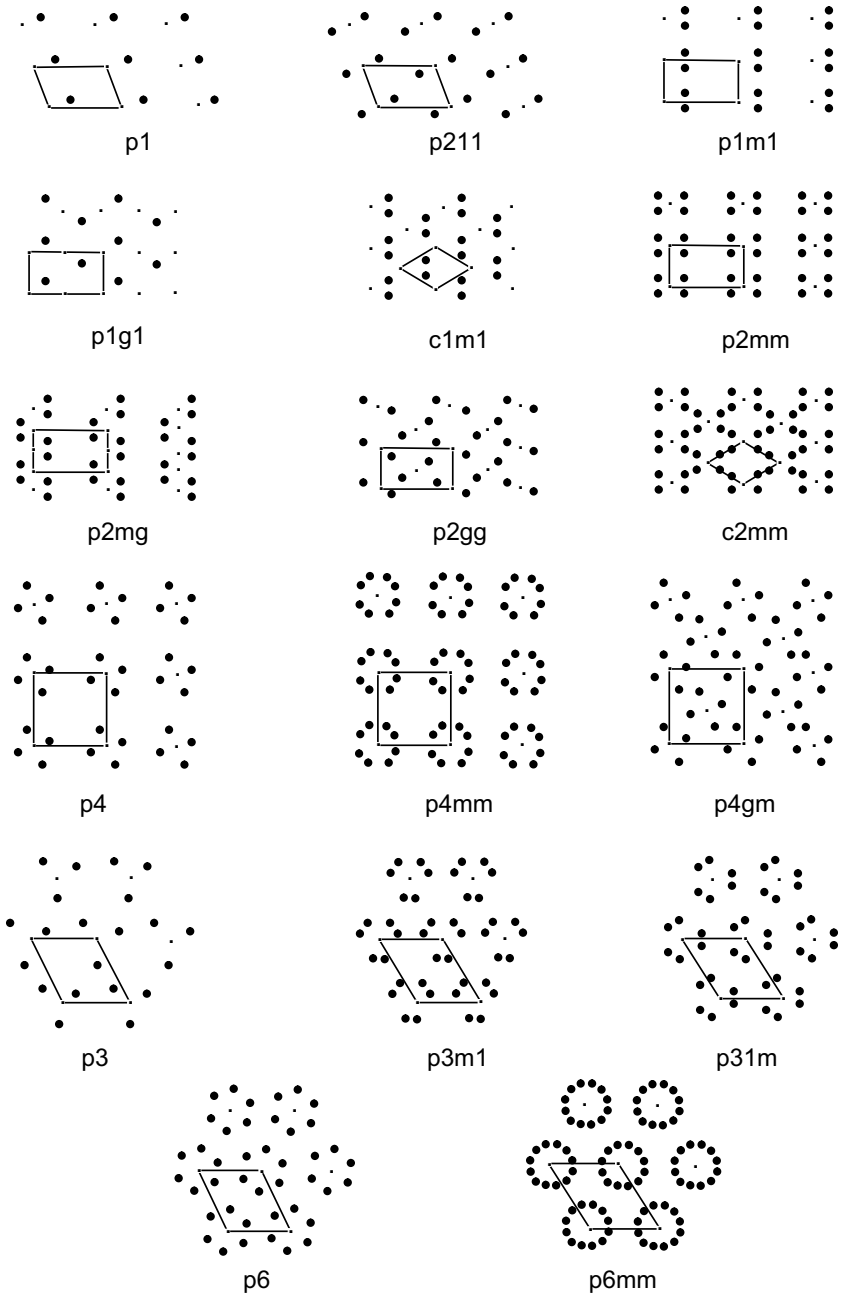

Fig. 1.16. The 17 planar space groups represented as parts of lattices satisfying the symmetries of those space groups. The small dots are at the corners of the unit cells, or at their midpoints, for reference. One large dot is positioned at an arbitrary non-symmetrical location within the unit cell, and the other large dots are obtained from this one by applying all the relevant symmetry operations. After [1.7].

Table 1.3. Symmetry classification of two-dimensional crystals [1.2, 1.10].

Crystal system	Bravais class	Point group	Space group	Symmetry elements
oblique	p-oblique	1	$p1$	$\{\varepsilon\|\boldsymbol{R}\}$
2		2	$p211$	$\{\varepsilon\|\boldsymbol{R}\}$, $\{\delta_2^1\|\boldsymbol{R}\}$
rect-angular	p-rect-angular	m	$p1m1$	$\{\varepsilon\|\boldsymbol{R}\}$, $\{m_y\|\boldsymbol{R}\}$
$2mm$			$p1g1$	$\{\varepsilon\|\boldsymbol{R}\}$, $\{m_y\|\boldsymbol{\tau}+\boldsymbol{R}\}$, $\boldsymbol{\tau}=\frac{a_1}{2}\boldsymbol{e}_x$
		$2mm$	$p2mm$	$\{\varepsilon\|\boldsymbol{R}\}$, $\{\delta_2^1\|\boldsymbol{R}\}$, $\{m_y\|\boldsymbol{R}\}$, $\{m_x\|\boldsymbol{R}\}$
			$p2mg$	$\{\varepsilon\|\boldsymbol{R}\}$, $\{\delta_2^1\|\boldsymbol{R}\}$, $\{m_x\|\boldsymbol{\tau}+\boldsymbol{R}\}$, $\{m_y\|\boldsymbol{\tau}+\boldsymbol{R}\}$, $\boldsymbol{\tau}=\frac{a_1}{2}\boldsymbol{e}_x$
			$p2gg$	$\{\varepsilon\|\boldsymbol{R}\}$, $\{\delta_2^1\|\boldsymbol{R}\}$, $\{m_x\|\boldsymbol{\tau}+\boldsymbol{R}\}$, $\{m_y\|\boldsymbol{\tau}+\boldsymbol{R}\}$, $\boldsymbol{\tau}=\frac{a_1}{2}\boldsymbol{e}_x+\frac{a_2}{2}\boldsymbol{e}_y$
	c-rect-angular	m	$c1m1$	$\{\varepsilon\|\boldsymbol{R}\}$, $\{m_y\|\boldsymbol{R}\}$
		$2mm$	$c2mm$	$\{\varepsilon\|\boldsymbol{R}\}$, $\{m_x\|\boldsymbol{R}\}$, $\{m_y\|\boldsymbol{R}\}$, $\{\delta_2^1\|\boldsymbol{R}\}$
square	p-square	4	$p4$	$\{\varepsilon\|\boldsymbol{R}\}$, $\{\delta_4^1\|\boldsymbol{R}\}$, $\{\delta_4^2\|\boldsymbol{R}\}$, $\{\delta_4^3\|\boldsymbol{R}\}$
$4mm$		$4mm$	$p4mm$	$\{\varepsilon\|\boldsymbol{R}\}$, $\{\delta_4^1\|\boldsymbol{R}\}$, $\{\delta_4^2\|\boldsymbol{R}\}$, $\{\delta_4^3\|\boldsymbol{R}\}$, $\{m_x\|\boldsymbol{R}\}$, $\{m_y\|\boldsymbol{R}\}$, $\{m_d\|\boldsymbol{R}\}$, $\{m_d'\|\boldsymbol{R}\}$
			$p4gm$	$\{\varepsilon\|\boldsymbol{R}\}$, $\{\delta_4^1\|\boldsymbol{R}\}$, $\{\delta_4^2\|\boldsymbol{R}\}$, $\{\delta_4^3\|\boldsymbol{R}\}$, $\{m_x\|\boldsymbol{\tau}+\boldsymbol{R}\}$, $\{m_y\|\boldsymbol{\tau}+\boldsymbol{R}\}$, $\{m_d\|\boldsymbol{R}+\boldsymbol{\tau}\}$, $\{m_d'\|\boldsymbol{R}+\boldsymbol{\tau}\}$, $\boldsymbol{\tau}=\frac{a}{2}(\boldsymbol{e}_x+\boldsymbol{e}_y)$
hexa-gonal	p-hexa-gonal	3	$p3$	$\{\varepsilon\|\boldsymbol{R}\}$, $\{\delta_3^1\|\boldsymbol{R}\}$, $\{\delta_3^2\|\boldsymbol{R}\}$
$6mm$		$3m$	$p3m1$	$\{\varepsilon\|\boldsymbol{R}\}$, $\{\delta_3^1\|\boldsymbol{R}\}$, $\{\delta_3^2\|\boldsymbol{R}\}$, $\{m_x\|\boldsymbol{R}\}$, $\{m_2\|\boldsymbol{R}\}$, $\{m_2'\|\boldsymbol{R}\}$
		6	$p31m$	$\{\varepsilon\|\boldsymbol{R}\}$, $\{\delta_3^1\|\boldsymbol{R}\}$, $\{\delta_3^2\|\boldsymbol{R}\}$, $\{m_y\|\boldsymbol{R}\}$, $\{m_1\|\boldsymbol{R}\}$, $\{m_1'\|\boldsymbol{R}\}$
			$p6$	$\{\varepsilon\|\boldsymbol{R}\}$, $\{\delta_6^1\|\boldsymbol{R}\}$, $\{\delta_6^2\|\boldsymbol{R}\}$, $\{\delta_6^3\|\boldsymbol{R}\}$, $\{\delta_6^4\|\boldsymbol{R}\}$, $\{\delta_6^5\|\boldsymbol{R}\}$
		$6mm$	$p6mm$	$\{\varepsilon\|\boldsymbol{R}\}$, $\{\delta_6^1\|\boldsymbol{R}\}$, $\{\delta_6^2\|\boldsymbol{R}\}$, $\{\delta_6^3\|\boldsymbol{R}\}$, $\{\delta_6^4\|\boldsymbol{R}\}$, $\{\delta_6^5\|\boldsymbol{R}\}$, $\{m_x\|\boldsymbol{R}\}$, $\{m_2\|\boldsymbol{R}\}$, $\{m_2'\|\boldsymbol{R}\}$, $\{m_y\|\boldsymbol{R}\}$, $\{m_1\|\boldsymbol{R}\}$, $\{m_1'\|\boldsymbol{R}\}$

Table 1.4. Space groups of ideal low-index surfaces of diamond-, zinc-blende-, and wurtzite-type crystals.

3D crystal structure	Surface	Space groups			
		First layer	First two layers	First three layers	Infinite half space
diamond	(111)	$p6mm$	$p3m1$	$p3m1$	$p3m1$
	(110)	$p2mg$	$p2mg$	$p2mg$	$p2mg$
	(100)	$p4mm$	$p2mm$	$p2mm$	$p2mm$
zinc blende	(111)	$p6mm$	$p3m1$	$p3m1$	$p3m1$
	(110)	$p1m1$	$p1m1$	$p1m1$	$p1m1$
	(100)	$p4mm$	$p2mm$	$p2mm$	$p2mm$
wurtzite	(0001)	$p6mm$	$p3m1$	$p3m1$	$p3m1$
	$(10\bar{1}1)$	$p2mm$	$p2mm$	$p1m1$	$p1m1$
	$(11\bar{2}0)$	$p2mm$	$p2mm$	$p1m1$	$p1m1$

Space groups of reconstructed low-index surfaces of diamond-type crystals

Surface	Model of reconstruction	Space groups		
		First layer	First two layers	Infinite half space
(111)2×1	buckling	$p2mm$	$p1m1$	$p1m1$
	π-bonded chain	$p2mg$	$p1m1$	$p1m1$
	π-bonded buckled chain	$p1m1$	$p1m1$	$p1m1$
	π-bonded molecule	$p2mm$	$p1m1$	$p1m1$
(100)2×1	symmetric dimer	$p2mm$	$p2mm$	$p2mm$
	asymmetric dimer	$p1m1$	$p1m1$	$p1m1$

ing the reconstruction is dropped in the following. The corresponding plane lattice constants are a_1 and a_2.

The general classification of 2D crystals in Table 1.3 can be used to characterize the symmetry of surfaces of real crystals. Examples are given in Table 1.4. This table indicates the space groups of low-index surfaces of typical semiconductors crystallizing in diamond, zinc-blende, or wurtzite structures. Ideal and reconstructed surfaces are considered and the resulting groups are discussed for different numbers of atomic layers below the uppermost one. Table 1.4 clearly shows that the resulting space group depends on the crystal

orientation, the number of atomic layers taken into account, and the model of reconstruction. That means, the space group of a 2D system depends on all of the above-mentioned details.

1.3 Reciprocal Space

1.3.1 Direct and Reciprocal Lattices

A two-dimensional solid surface is characterized by a 2D Bravais lattice (cf. Table 1.3) with primitive basis vectors $\bar{\boldsymbol{a}}_1$ and $\boldsymbol{a}_2$. We use the vectors with only one bar independent of whether or not a reconstruction is present. In terms of a rectangular planar Cartesian coordinate system with unit vectors $\boldsymbol{e}_x$ and $\boldsymbol{e}_y$, the basis vectors read as

$$\begin{aligned} \bar{\boldsymbol{a}}_1 &= A_{11}\boldsymbol{e}_x + A_{12}\boldsymbol{e}_y, \\ \bar{\boldsymbol{a}}_2 &= A_{21}\boldsymbol{e}_x + A_{22}\boldsymbol{e}_y. \end{aligned} \tag{1.16}$$

The determinant $\det \hat{A}$ of the 2×2 matrix

$$\hat{A} = \begin{pmatrix} A_{11} & A_{12} \\ A_{21} & A_{22} \end{pmatrix} \tag{1.17}$$

gives the area A of the unit cell of the Bravais lattice. In fact $A = \boldsymbol{n} \cdot (\bar{\boldsymbol{a}}_1 \times \bar{\boldsymbol{a}}_2) = \det \hat{A}$ with $\boldsymbol{n}$ as the surface normal.

A corresponding *reciprocal lattice* in Fourier space is associated with the Bravais lattice in real space. The reciprocal lattice, as we shall see throughout the book, is extremely useful and pertinent in all diffraction methods, in particular in the case of low-energy electron diffraction (LEED). As in three-dimensional space, the primitive basis vectors $\bar{\boldsymbol{b}}_1$ and $\boldsymbol{b}_2$ of the 2D reciprocal lattice are defined according to the orthogonality relation

$$\bar{\boldsymbol{a}}_i \cdot \bar{\boldsymbol{b}}_j = 2\pi\delta_{ij} \qquad (i, j = 1, 2). \tag{1.18}$$

With $\boldsymbol{n}$ as the unit vector normal to the surface, solutions of the relation (1.18) are

$$\bar{\boldsymbol{b}}_1 = 2\pi \frac{\bar{\boldsymbol{a}}_2 \times \boldsymbol{n}}{|\bar{\boldsymbol{a}}_1 \times \bar{\boldsymbol{a}}_2|}, \quad \bar{\boldsymbol{b}}_2 = 2\pi \frac{\boldsymbol{n} \times \bar{\boldsymbol{a}}_1}{|\bar{\boldsymbol{a}}_1 \times \bar{\boldsymbol{a}}_2|}. \tag{1.19}$$

The lengths of these vectors are $|\bar{\boldsymbol{b}}_i| = 2\pi / [a_i \sin(\bar{\boldsymbol{a}}_1, \bar{\boldsymbol{a}}_2)]$. The primitive basis vectors can be used to construct the reciprocal lattice to a given 2D network. This is schematically shown in Fig. 1.17. A general translational vector in reciprocal space is given by

$$\boldsymbol{g}_{hk} = h\bar{\boldsymbol{b}}_1 + k\bar{\boldsymbol{b}}_2, \tag{1.20}$$

where h and k are integers. The set of all vectors $\boldsymbol{g}_{hk}$ gives the reciprocal net.

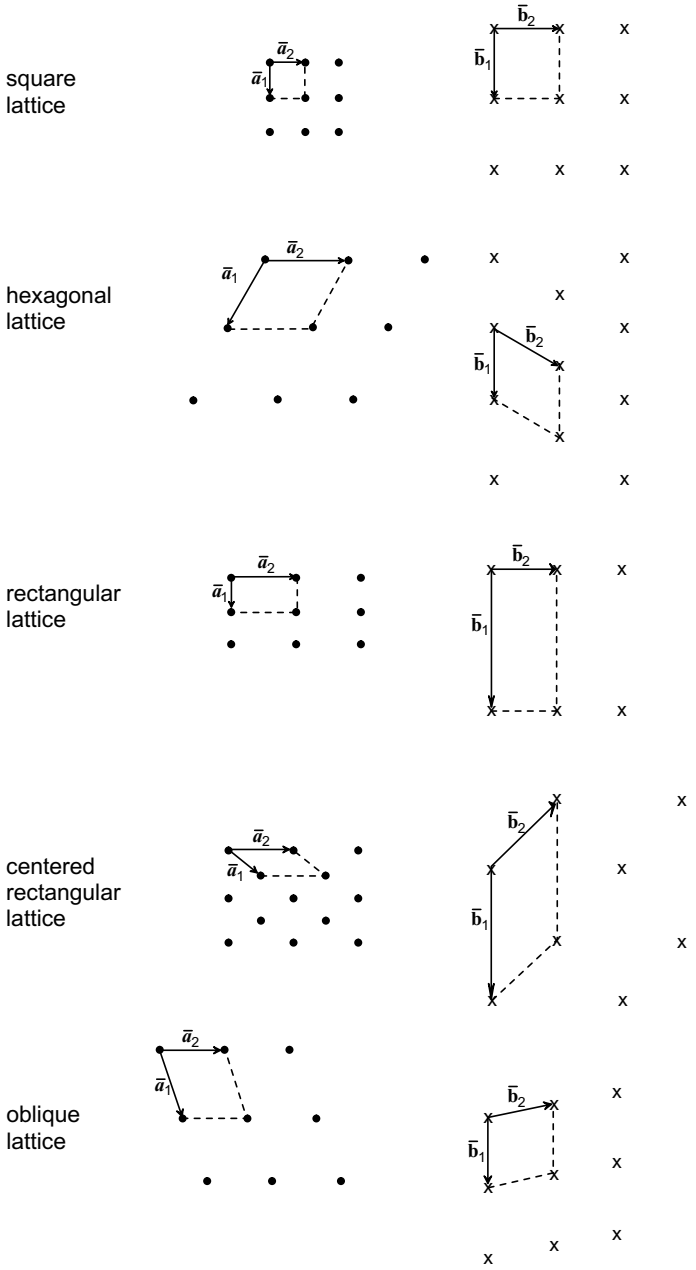

Fig. 1.17. Direct lattice (left) and corresponding reciprocal lattice (right). The five 2D Bravais lattices are presented.

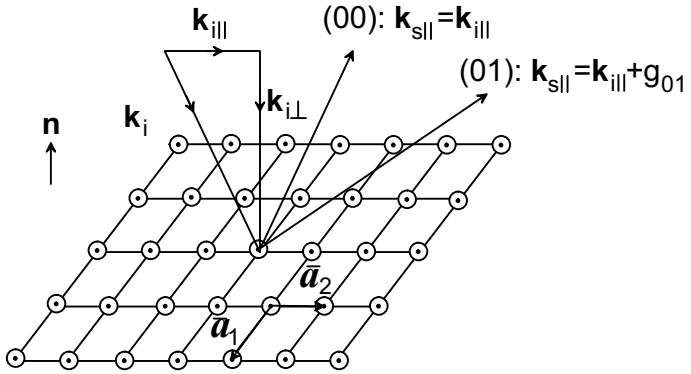

Fig. 1.18. Diffraction of an incident plane wave with wave vector $\boldsymbol{k}_\mathrm{i}$. The surface is represented by the corresponding 2D Bravais lattice. Parallel momentum conservation with any reciprocal lattice vector $\boldsymbol{g}_{hk}$ creates well-defined diffracted beams (hk).

The reciprocal lattice vectors have a direct physical meaning. In a diffraction experiment, e.g., LEED, each diffracted beam corresponds to a reciprocal lattice vector $\boldsymbol{g}_{hk}$ and, in fact, each such beam can be labeled by the values h and k as the beam (hk). This is indicated schematically in Fig. 1.18. The angle of emergence of the diffracted beams is determined by the conservation law of the linear momentum parallel to the surface. The momentum of inci-

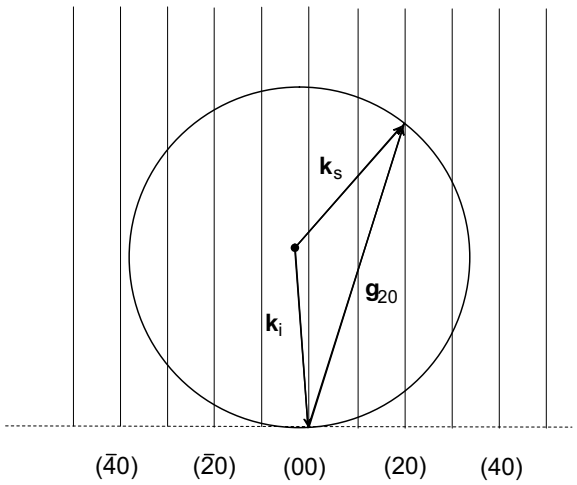

Fig. 1.19. Ewald construction for elastic scattering on a 2D Bravais lattice. A scattering geometry is considered in which the momentum conservation is fulfilled with reciprocal lattice vectors $\boldsymbol{g}_{h0}$ parallel to $\bar{\boldsymbol{b}}_1$.

Table 1.5. Direct and reciprocal lattices of two-dimensional crystals.

Bravais class	$\bar{a}_1$, $\bar{a}_2$	Unit cell of direct lattice	$\bar{b}_1$, $\bar{b}_2$	Brillouin zone
oblique	$(a_{1x}, 0)$ (a_{2x}, a_{2y})	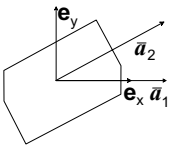	$\frac{2\pi}{a_{1x}}(1, -\frac{a_{2x}}{a_{2y}})$ $\frac{2\pi}{a_{2y}}(0, 1)$	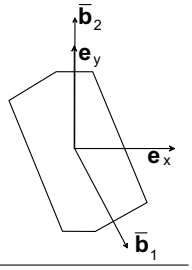
p-rectangular	$(a_1, 0)$ $(0, a_2)$	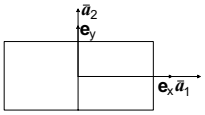	$\frac{2\pi}{a_1}(1, 0)$ $\frac{2\pi}{a_2}(0, 1)$	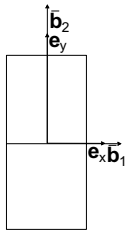
c-rectangular	$(\frac{a_1}{2}, -\frac{a_2}{2})$ $(\frac{a_1}{2}, \frac{a_2}{2})$	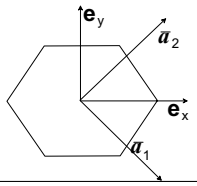	$\frac{2\pi}{a_1}(1, -\frac{a_1}{a_2})$ $\frac{2\pi}{a_1}(1, \frac{a_1}{a_2})$	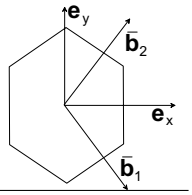
square	$(a, 0)$ $(0, a)$	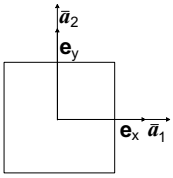	$\frac{2\pi}{a}(1, 0)$ $\frac{2\pi}{a}(0, 1)$	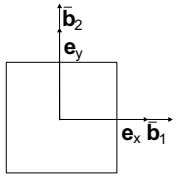
hexagonal	$(a, 0)$ $\frac{a}{2}(1, \sqrt{3})$	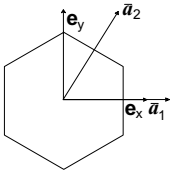	$\frac{2\pi}{a}(1, -\frac{1}{\sqrt{3}})$ $\frac{2\pi}{a}(0, \frac{2}{\sqrt{3}})$	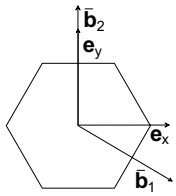

dent particles is $\boldsymbol{p} = \hbar \boldsymbol{k}_\mathrm{i}$, where $\boldsymbol{k}_\mathrm{i}$ is the wave vector. With $\boldsymbol{k}_\mathrm{s}$ as the wave vector of the diffracted particles the momentum conservation reads as

$$\boldsymbol{k}_{\mathrm{s}||} = \boldsymbol{k}_{\mathrm{i}||} + \boldsymbol{g}_{hk}. \tag{1.21}$$

After the diffractive scattering the parallel component of the momentum may be equal to that of the incident particle (e.g. an electron) beam, i.e., $\boldsymbol{g}_{hk} = 0$. There is no relation between the components of $\boldsymbol{k}_s$ and $\boldsymbol{k}_\mathrm{i}$ perpendicular to the surface, because there is no translational symmetry in this direction. However, the particles studied in a diffraction experiment, e.g., the electrons in the LEED case, are elastically scattered. One therefore has

$$|\boldsymbol{k}_\mathrm{s}| = |\boldsymbol{k}_\mathrm{i}|. \tag{1.22}$$

A solution of the two equations (1.21) and (1.22) always exists for given vectors $\boldsymbol{k}_\mathrm{i}$ and $\boldsymbol{g}_{hk}$. This is in contrast to the case of scattering of particles from bulk crystals with 3D translational symmetry. Coherent scattering can only occur if $\boldsymbol{k}_\mathrm{i}$ lies on a Bragg reflection plane. The solution of the above equations can be readily carried out using the Ewald construction shown in Fig. 1.19. The points, at which the vertical lines passing through the reciprocal lattice points $\boldsymbol{g}_{hk}$ intersect the sphere $|\boldsymbol{k}_\mathrm{s}| = |\boldsymbol{k}_\mathrm{i}|$, determine the directions in which diffraction maxima occur. There is exactly one maximum for each reciprocal lattice vector. The reciprocal surface lattice can thus be read from the diffraction maxima on the LEED registration screen. The relation between the direct lattice and the reciprocal lattice for the five 2D Bravais nets is shown explicitly in Fig. 1.17. The direct relationships between the direct and reciprocal lattices of 2D systems are given in Table 1.5 in terms of a two-dimensional Cartesian coordinate system defined by the vectors $\boldsymbol{e}_x$ and $\boldsymbol{e}_y$. In more detail, the table relates the primitive basis vectors $\bar{\boldsymbol{a}}_1$, $\bar{\boldsymbol{a}}_2$ and $\bar{\boldsymbol{b}}_1$, $\bar{\boldsymbol{b}}_2$ to the Cartesian vectors using the lattice constants a_1, a_2 (or $a_1 = a_2 = a$) of the 2D nets. Moreover, the relationship between the Wigner–Seitz cells of the direct lattice (i.e., the unit cell) and the reciprocal lattice (i.e., the Brillouin zone) is presented.

Typical LEED images are presented for rectangular (square) lattices in Fig. 1.20 and for hexagonal lattices in Fig. 1.21. The bright spots correspond to the reciprocal lattice of the ideal surface, while the less bright spots are related to the finer reciprocal lattice of the reconstructed surface. One has to mention that the construction in Fig. 1.19 is exact only in the limit of scattering from a true 2D network of atoms. In a real electron diffraction experiment, however, the primary electrons penetrate several atomic layers into the solid. Therefore, the mean free path of electrons determines how the third Laue condition becomes more and more important. This leads to a modulation of the intensities of the Bragg reflections in comparison with the case of pure 2D scattering.

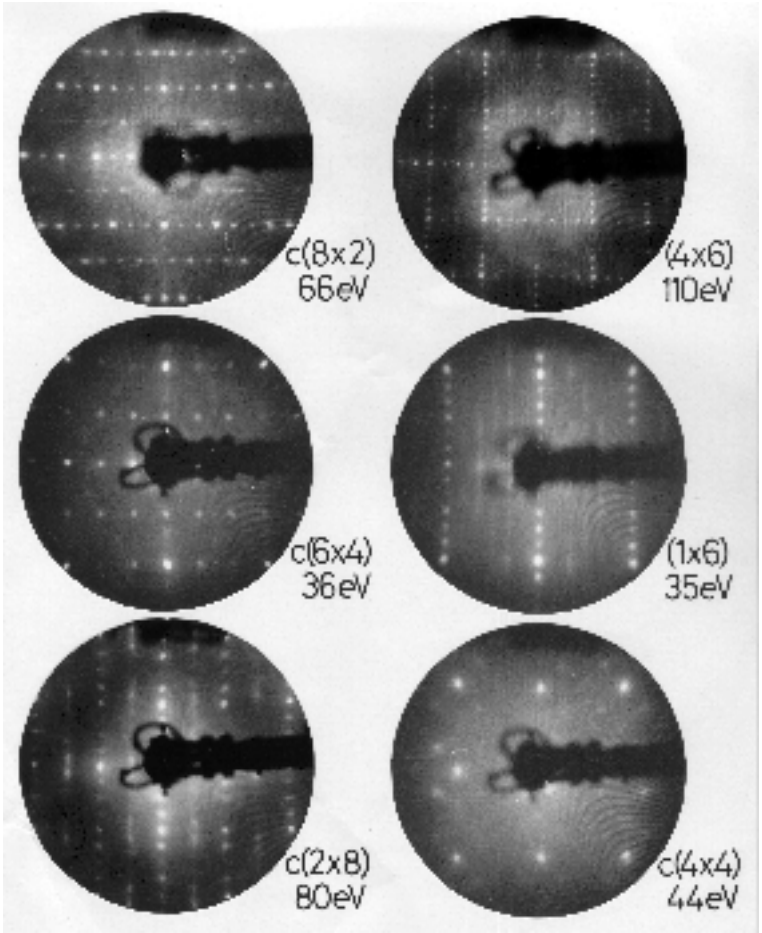

Fig. 1.20. LEED images of six differently prepared GaAs(100) surfaces. After [1.15]. The surface reconstruction and the electron energy are indicated.

1.3.2 Brillouin Zones

In translationally invariant systems the wave vector $\boldsymbol{k}$ defines a set of 'good' quantum numbers for each type of elementary excitation. In the case of an ordered surface of a crystal, such a wave vector, $\bar{\boldsymbol{k}}$, is restricted to two dimensions, i.e., is parallel to the surface. Within a reduced zone scheme it is restricted to a 2D Brillouin zone (BZ). The entire 2D reciprocal space can be covered by the vectors $\bar{\boldsymbol{k}} + \boldsymbol{g}$, where $\boldsymbol{g}$ is a surface reciprocal lattice vector (1.20). The surface BZ is defined as the smallest polygon in the 2D reciprocal space situated symmetrically with respect to a given lattice point (used as

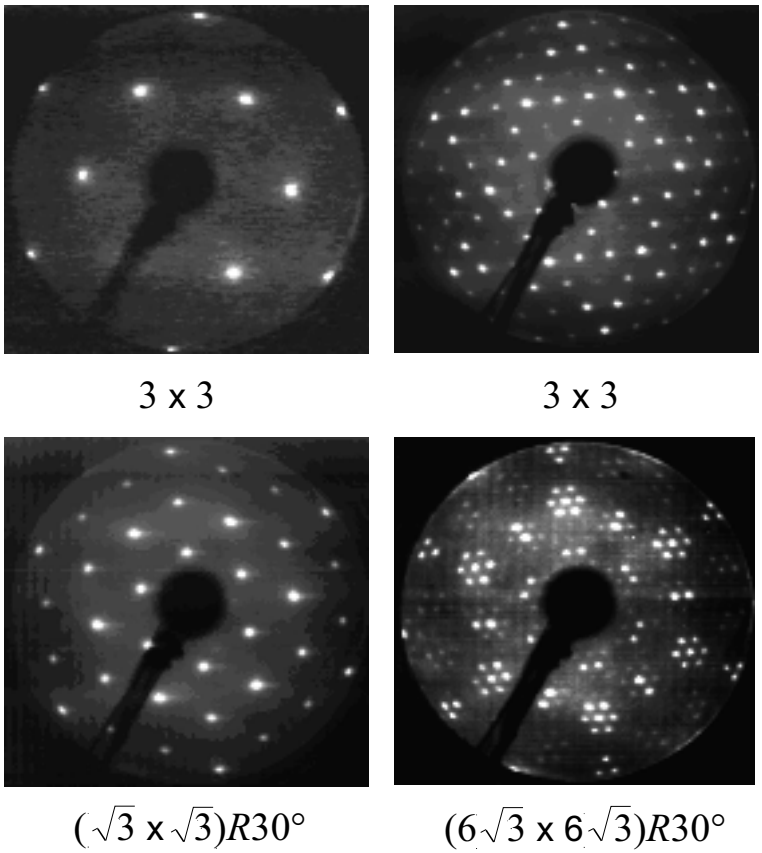

Fig. 1.21. Sequence of LEED patterns (with almost the same electron energy ≈ 130 eV) for the Si-terminated surface of 6H-SiC(0001). The 1×1 bulk-terminated phase is stabilized by OH adsorption, whereby the following reconstructed surfaces result by 800 °C annealing of the latter in Si-flux (3×3 phase) followed by annealing at about 1000 °C ($(\sqrt{3}\times\sqrt{3})R30^\circ$ phase) and at 1100 °C ($(6\sqrt{3}\times 6\sqrt{3})R30^\circ$ phase) [courtesy of J. Bernhardt, U. Starke and K. Heinz (University of Erlangen)].

coordinate zero) and bounded by points $\bar{\boldsymbol{k}}$ satisfying the equation

$$\bar{\boldsymbol{k}} \cdot \boldsymbol{g} = \frac{1}{2}|\boldsymbol{g}|^2. \tag{1.23}$$

The set of points defined by (1.23) gives a straight line at a distance $|\boldsymbol{g}|/2$ from the zero point which bisects the connection to the next lattice point $\boldsymbol{g}$ at right angles.

Since there are five different plane Bravais lattices and, hence, five different reciprocal surface lattices, there are also five different 2D or surface Brillouin zones. They are shown in Fig. 1.22. Their shapes are the same as those of the Wigner–Seitz cells of the corresponding direct lattices (cf. Table 1.5), since

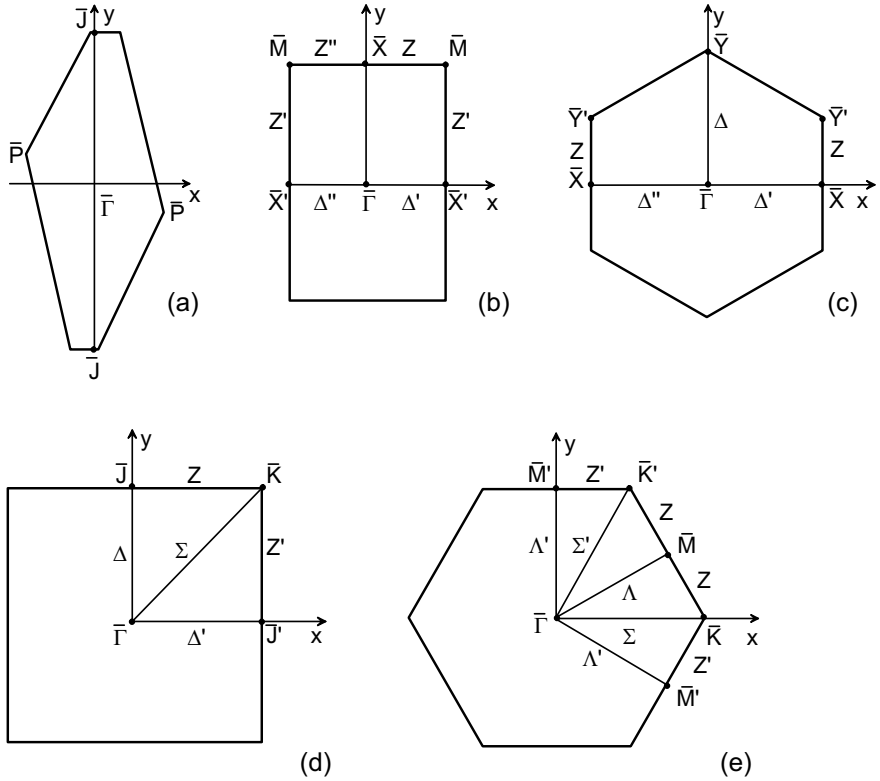

Fig. 1.22. Brillouin zones of the five plane lattices: (a) oblique, (b) *p*-rectangular, (c) *c*-rectangular, (d) square, and (e) hexagonal. Symmetry lines and points are also shown, and their notations are introduced. The 2D Cartesian coordinate system is chosen so that the point symmetry operations in Table 1.3 can be directly applied.

the Bravais types of the direct and reciprocal surface lattices always coincide. In Fig. 1.22 we have labeled some of the high-symmetry points of the Brillouin zones using letters $\bar{X}$ and $\bar{\Gamma}$. The bar indicates such points in 2D Brillouin zones whereas points like X and Γ indicate positions in the corresponding 3D Brillouin zone of infinite 3D crystals. We follow the convention of denoting high symmetry points and lines *inside* the BZ by Greek letters, e.g., $\bar{\Gamma}$ and Δ, Λ, Σ. Points and lines on the *boundary* of the BZ are denoted by Roman letters, e.g., $\bar{M}$ and Z. The center of the BZ is always denoted by $\bar{\Gamma}$. Apart from the hexagonal Bravais system the high-symmetry lines parallel to the axes of the 2D Cartesian coordinate system are indicated by the Greek letter Δ. In the hexagonal case, Σ or Λ is used to indicate a line from $\bar{\Gamma}$ to a corner point of the hexagon or a midpoint on an edge. The primes on the Greek or Roman letters are used to allow an indication of different symmetries in cases where the point group of the 2D crystal is only a subgroup of the holohedral group of the Bravais lattice.

Unfortunately, the notation in the literature is not consistent. In the original papers several modifications are used. Which of the different points should be indicated by a prime or not, is not exactly fixed. For instance, sometimes in papers about the cleavage face of zinc-blende crystals or the (110)1×1 surface of group-IV crystals, $\bar{\Gamma}\bar{X}$ is used to indicate the shorter axis in the BZ, in contrast to Fig. 1.22 where this line is denoted by $\bar{\Gamma}\bar{X}'$. There are also examples where authors use the notation $\bar{Y}$ instead of $\bar{X}'$ [1.11]. In the case of the 2×1 reconstructed (111) and (100) surfaces of group-IV materials, there is a tradition of following the notation of the square lattice. Instead of $\bar{X}$ and $\bar{M}$, the notation $\bar{J}$ and $\bar{K}$ is used [1.12, 1.13]. In the latter case even $\bar{J}$ and $\bar{J}'$ are interchanged. Sometimes one finds a paper in which the corner of the BZ is denoted by $\bar{S}$ and the midpoint of the edge of the rectangle by $\bar{Y}$ [1.14].

1.3.3 Projection of 3D Onto 2D Brillouin Zones

The fact that the 3D wave vector $\boldsymbol{k}$ from the BZ gives a set of 'good' quantum numbers for elementary excitations in an infinite crystal has several consequences for the representation of the energy spectrum of elementary excitations in a crystal with surface. On the one hand, bulk excitations should also occur in a semi-infinite halfspace with surface. On the other hand, such a system is only characterized by a 2D translational symmetry. Consequently, the elementary excitations of the finite system can only be characterized by wave vectors $\bar{\boldsymbol{k}}$ from the Brillouin zone belonging to the corresponding 2D Bravais lattice. In order to use the Bloch-like eigenvalues of a bulk elementary excitation, the relationship between the eigenvalue of the bulk crystal and the wave vector has to be altered. To represent all allowed eigenstates, usually the component $\boldsymbol{k}_{||}$ of the 3D vector parallel to the surface can be fixed, while the perpendicular component $\boldsymbol{k}_{\perp}$ has to be varied. Generally speaking, the bulk eigenvalue must be assigned to a 2D wave vector $\bar{\boldsymbol{k}}$ in the surface BZ instead of a 3D wave vector $\boldsymbol{k}$ in the bulk BZ. For obvious reasons, such a relationship is called a projection of the Bloch-like eigenvalues of the bulk crystal, the 3D dispersion relations, onto the surface BZ.

Within an explicit procedure certain bulk directions and points of high symmetry in the 3D Brillouin zone are projected onto the 2D surface BZ. For three 3D Bravais lattices and some low-index surfaces the relation is depicted in Figs. 1.23 – 1.25. In order to illustrate the projection procedure, first the Brillouin zones under consideration must be specified. The corresponding bulk BZ is defined by the Bragg reflection planes

$$\boldsymbol{k} \cdot \boldsymbol{G} = \frac{1}{2}|\boldsymbol{G}|^2, \tag{1.24}$$

where $\boldsymbol{G}$ is a certain vector of the reciprocal lattice of the bulk crystal. The surface BZ may be calculated according to (1.23). The primitive vectors $\bar{\boldsymbol{b}}_1$, $\bar{\boldsymbol{b}}_2$ of the reciprocal surface lattice needed in deriving this equation follow

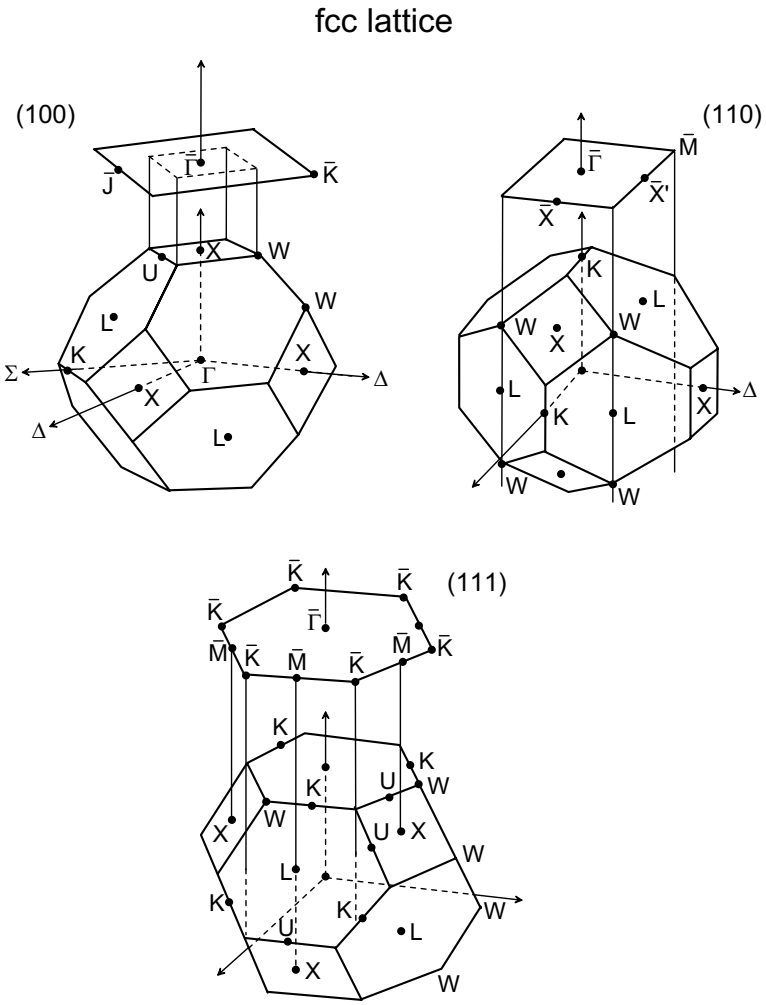

Fig. 1.23. Relation between 2D Brillouin zones of low-index surfaces and the 3D bulk BZ in the fcc case. After [1.16].

from (1.19) using the primitive vectors $\bar{\boldsymbol{a}}_1$, $\bar{\boldsymbol{a}}_2$ of the direct surface lattice considered. Such vectors are given in Table 1.5 for all 2D systems. Second, the bulk BZ is projected onto the plane of the surface BZ as indicated in Figs. 1.23 – 1.25. We denote by $\boldsymbol{k}_{||}$ the component of a wave vector $\boldsymbol{k}$ of the bulk BZ parallel to the surface. The boundary points of the projected bulk BZ are located on straight lines determined by the two equations

$$\begin{aligned} &\boldsymbol{k}_{||} = k_{||1}\bar{\boldsymbol{b}}_1 + k_{||2}\bar{\boldsymbol{b}}_2, \\ &\boldsymbol{k}_{||} \cdot \boldsymbol{G} = \frac{1}{2}|\boldsymbol{G}|^2. \end{aligned} \tag{1.25}$$

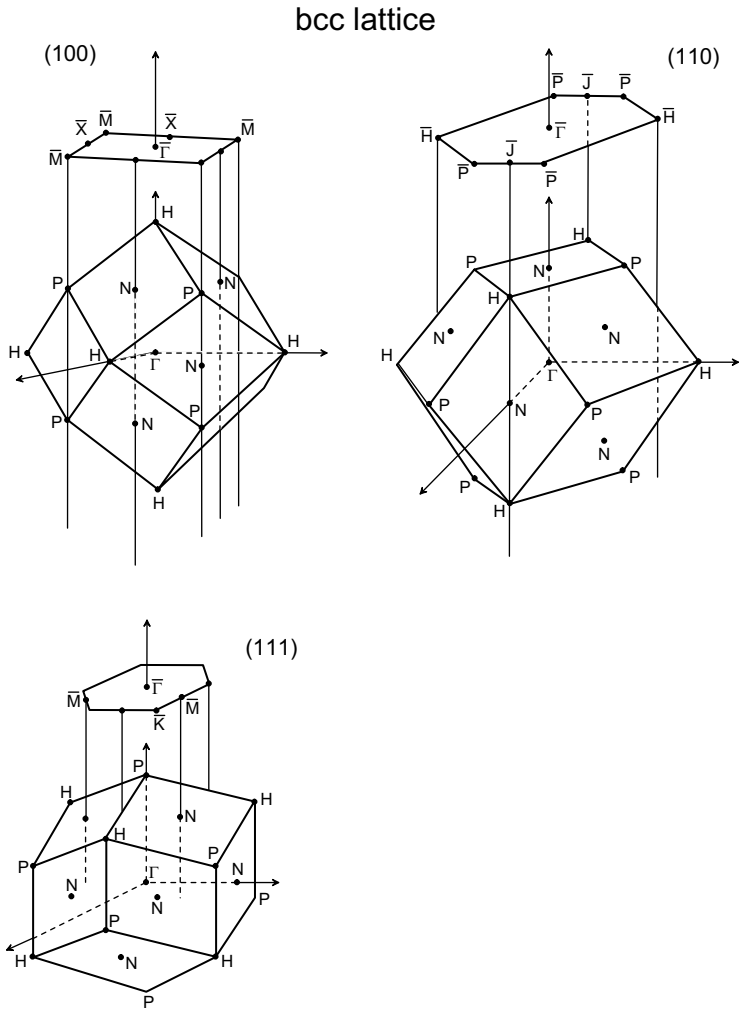

Fig. 1.24. Relation between 2D Brillouin zones of low-index surfaces and the 3D bulk BZ in the bcc case. After [1.16].

In general, the projected bulk BZ does not coincide with one surface BZ. It is usually larger (see e.g. in Fig. 1.26 the example of the (100) surface of an fcc crystal), and one has to fold back the part of the projected bulk BZ not contained in the surface BZ onto the latter one. Since these parts of the projected bulk BZ agree with neighboring 2D Brillouin zones belonging to reciprocal lattice vectors $\boldsymbol{g}(\boldsymbol{k}_{||})$, the folding is identical with a displacement by $\boldsymbol{g}(\boldsymbol{k}_{||})$. Consequently, all wave vectors $\bar{\boldsymbol{k}}$ in the surface BZ are given by

$$\bar{\boldsymbol{k}} = \boldsymbol{k}_{||} + \boldsymbol{g}(\boldsymbol{k}_{||}). \tag{1.26}$$

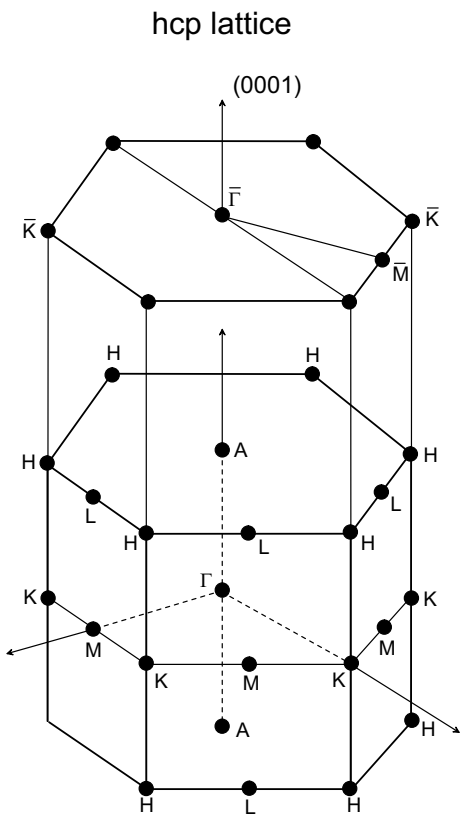

Fig. 1.25. Relation between the 2D Brillouin zone of the (0001) surfaces and the 3D BZ of a hcp structure. After [1.16].

In this manner certain regions of the surface BZ are covered two or more times by projected points of the bulk BZ.

We elucidate the above general considerations, using as an example the (100) surface of an fcc crystal. The 14 vectors of the reciprocal lattice defining the bulk BZ according to (1.24) are $\boldsymbol{G} = \frac{2\pi}{a}(\pm\boldsymbol{e}_x \pm \boldsymbol{e}_y \pm \boldsymbol{e}_z)$ and $\boldsymbol{G} = \pm\frac{4\pi}{a}\boldsymbol{e}_{x,y,z}$. The primitive vectors of the reciprocal surface lattice are $\bar{\boldsymbol{b}}_1 = \frac{2\pi}{a}(\boldsymbol{e}_y - \boldsymbol{e}_z)$ and $\bar{\boldsymbol{b}}_2 = \frac{2\pi}{a}(\boldsymbol{e}_y + \boldsymbol{e}_z)$. The four vectors defining the surface BZ are $\boldsymbol{g} = \pm\bar{\boldsymbol{b}}_1, \pm\bar{\boldsymbol{b}}_2$. According to (1.25)

$$k_{||1}(\boldsymbol{e}_y - \boldsymbol{e}_z)\boldsymbol{G} + k_{||2}(\boldsymbol{e}_y + \boldsymbol{e}_z)\boldsymbol{G} = \frac{a}{4\pi}|\boldsymbol{G}|^2. \tag{1.27}$$

If $\boldsymbol{G} = \frac{2\pi}{a}(\boldsymbol{e}_x + \boldsymbol{e}_y + \boldsymbol{e}_z)$, for example, is chosen, it follows that

$$k_{||2} = \frac{3}{4}, \tag{1.28}$$

and

$$k_{||1} + k_{||2} = 1, \tag{1.29}$$

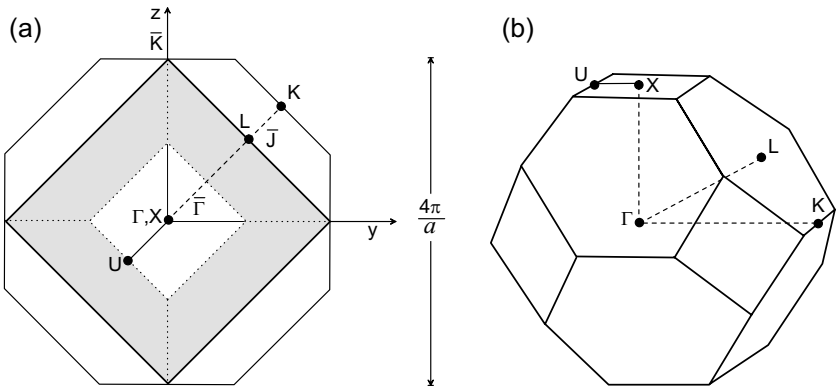

Fig. 1.26. (a) Brillouin zone of a (100) surface (shaded area) together with the projected bulk BZ of an fcc crystal. Projected critical points of the 3D BZ are indicated along a [011] direction. (b) Bulk BZ for comparison.

if $\boldsymbol{G} = \frac{4\pi}{a}\boldsymbol{e}_y$. For the other vectors of the 3D reciprocal lattice, either similar relations result or the associated Bragg reflection planes are parallel to the plane of the surface BZ (and thus do not intersect it). The evaluation of the relations of type (1.28) and (1.29) results in Fig. 1.26a. One notes that the trapezoidal areas of the projected fcc BZ lying outside the surface BZ can be folded over the surface BZ by displacements along one of the lattice vectors $\bar{\boldsymbol{b}}_1$, $-\bar{\boldsymbol{b}}_1$, $\bar{\boldsymbol{b}}_2$, $-\bar{\boldsymbol{b}}_2$. The little square in the center is part of the Bragg reflection plane bounding the bulk BZ and associated with a reciprocal lattice vector $\boldsymbol{G} = \pm\frac{2\pi}{a}(1,0,0)$ perpendicular to the surface. The maximum (minimum) of $k_\perp (= k_x)$ is thus $\pm\frac{2\pi}{a}$. Outside the little square, $k_\perp = k_\perp(\boldsymbol{k}_{||})$ varies in a smaller interval fixed by the 3D BZ. The interval depends on the wave vector $\boldsymbol{k}_{||}$.

1.3.4 Symmetry of Points and Lines in Reciprocal Space

The spatial symmetry of a crystal with surface has implications for the possible degree of degeneracy of elementary excitations with energies $\hbar\Omega_\mu(\bar{\boldsymbol{k}})$. The eigenvalues $\Omega_\mu(\bar{\boldsymbol{k}})$ as a function of the 2D wave vector $\bar{\boldsymbol{k}}$ give the so-called dispersion relation for the corresponding elementary excitation. The set of indices μ labels the remaining quantum numbers. Examples are electron and hole excitations with $\Omega_\mu(\bar{\boldsymbol{k}})$ as the surface energy bands and μ as the band index, surface phonons with dispersion relations $\Omega_\mu(\bar{\boldsymbol{k}})$ of the vibrational branches μ, surface plasmons, etc.

The spatial symmetry results in relations between the values $\Omega_\mu(\bar{\boldsymbol{k}})$ for different $\bar{\boldsymbol{k}}$ values. The key for such conclusions are, in analogy to the infinite bulk case, the irreducible representations of the space group of the given crystal with surface. This is based on the fact that the eigenfunctions belonging to a particular energy eigenvalue form a basis set of an irreducible

Table 1.6. Point groups of the high-symmetry points and lines of the BZ [1.10]. The irreducible part of the BZ is indicated by the hatched region.

a) Oblique lattice

Symmetry point	Space group	
	$p1$	$p211$
$\bar{\Gamma}$	1	2
$\bar{J}$	1	2
Irreducible part of BZ	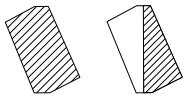	

b) p-rectangular lattice

Symmetry point	Space group				
or line	$p1m1$	$p1g1$	$p2mm$	$p2mg$	$p2gg$
$\bar{\Gamma}$	m	m	$2mm$	$2mm$	$2mm$
$\Delta'\Delta''$	m	m	m	m	m
$\bar{X}\bar{X}'$	m	m	$2mm$	$2mm$	$2mm$
Z'	–	–	m	m	m
$\bar{M}$	m	m	$2mm$	$2mm$	$2mm$
ZZ'	m	m	m	m	m
Δ	–	–	m	m	m
Irreducible part of BZ	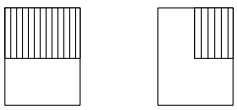				

representation of this group. Such a representation may be characterized by the star $\{\bar{\boldsymbol{k}}\}$ of the wave vector $\bar{\boldsymbol{k}}$ and the irreducible representations of the *small point group* of $\bar{\boldsymbol{k}}$ [1.10].

A small point group is a subgroup of the point group of the crystal. The point-group elements $\hat{\alpha}$ of such a subgroup transform $\bar{\boldsymbol{k}}$ neither into itself nor into a vector equivalent to $\bar{\boldsymbol{k}}$ that differs from $\bar{\boldsymbol{k}}$ only by a reciprocal lattice vector $\boldsymbol{g}$. The set of all different and non-equivalent vectors $\hat{\alpha}\bar{\boldsymbol{k}}$ is called *star* of $\bar{\boldsymbol{k}}$. At all points of the star $\{\bar{\boldsymbol{k}}\}$ the energy eigenvalues $\Omega_\mu(\bar{\boldsymbol{k}})$ have the same value. The small point groups of high-symmetry points and lines in the BZ are listed in Table 1.6 for the various space groups of Bravais lattices.

Table 1.6. (continued)

c) c-rectangular lattice

Symmetry point	Space group	
or line	$c1m1$	$c2mm$
$\bar{\Gamma}$	m	$2mm$
$\Delta'\Delta''$	m	m
$\bar{X}$	m	$2mm$
Z	–	m
$\bar{Y}'$	–	m
$\bar{Y}$	–	m
Δ	–	m
Irreducible part of BZ	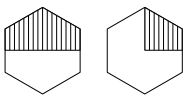	

d) Square lattice

Symmetry point	Space group		
or line	$p4$	$p4mm$	$p4mg$
$\bar{\Gamma}$	4	$4mm$	$4mm$
Δ	–	m	m
$\bar{J}$	2	$2mm$	$2mm$
Z	–	m	m
$\bar{K}$	4	$4mm$	$4mm$
Σ	–	m	m
Irreducible part of BZ	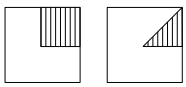		

Table 1.6. (continued)

e) Hexagonal lattice

Symmetry	Space group				
points or lines	$p3$	$p31m$	$p3m1$	$p6$	$p6mm$
$\bar{\Gamma}$	3	$3m$	$3m$	6	$6mm$
$\Sigma\Sigma'$	–	m	–	–	m
$\bar{M}\bar{M}'$	3	$3m$	3	3	$3m$
ZZ'	–	m	–	–	m
$\bar{K}\bar{K}'$	–	m	m	2	$2mm$
$\Lambda\Lambda'$	–	–	m	–	m
Irreducible part of BZ	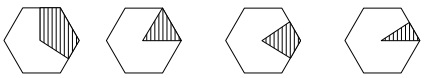				

The irreducible representations of these point groups are given in [1.10] for the various space groups of a corresponding Bravais lattice. The dimension of the irreducible representation determines the degeneracy of an eigenvalue at a given $\bar{\boldsymbol{k}}$. For the systems under consideration only irreducible representations with dimensions equal to 1 or 2 will appear.